AGU PUBLICATIONS

Tectonics

RESEARCH ARTICLE
10.1002/2015TC003997

Key Points:
- Paleoseismicity in the Eastern Betics Shear Zone (Carrascoy Fault SW segment)
- Migration of active faulting away from the main range (foreberg)
- Nine to 11 Mw ~6.7 events in the last 30.2 kyr and a slip rate of 0.37 m/kyr

Supporting Information:
- Tables S1–S5 captions
- Table S1
- Table S2
- Table S3
- Table S4
- Table S5

Correspondence to:
R. Martín-Banda,
raquem08@ucm.es

Citation:
Martín-Banda, R., J. García-Mayordomo, J. M. Insua-Arévalo, Á. E. Salazar, E. Rodríguez-Escudero, J. A. Álvarez-Gómez, A. Medialdea, and M. J. Herrero (2016), New insights on the seismogenic potential of the Eastern Betic Shear Zone (SE Iberia): Quaternary activity and paleoseismicity of the SW segment of the Carrascoy Fault Zone, *Tectonics*, *35*, 55–75, doi:10.1002/2015TC003997.

Received 10 AUG 2015
Accepted 24 NOV 2015
Accepted article online 26 NOV 2015
Published online 6 JAN 2016

New insights on the seismogenic potential of the Eastern Betic Shear Zone (SE Iberia): Quaternary activity and paleoseismicity of the SW segment of the Carrascoy Fault Zone

Raquel Martín-Banda[1], Julián García-Mayordomo[2], Juan M. Insua-Arévalo[1], Ángel E. Salazar[2], Emilio Rodríguez-Escudero[3], Jose A. Álvarez-Gómez[1], Alicia Medialdea[4], and María J. Herrero[5]

[1]Department of Geodynamics, Complutense University of Madrid, Madrid, Spain, [2]Geological and Mining Institute of Spain, Madrid, Spain, [3]Department of Geology and Geochemistry, Autónoma University of Madrid, Madrid, Spain, [4]Nordic Laboratory for Luminescence Dating, Department of Geoscience, Aarhus University, Aarhus, Denmark, [5]Department of Petrology and Geochemistry, Complutense University of Madrid, Madrid, Spain

Abstract The Carrascoy Fault (CAF) is one of the main active faults that form part of the Eastern Betic Shear Zone, a 450 km fault system that accommodates most of the convergence between the Eurasian (Iberia) and Nubian plates in the Betic Cordillera, south Spain. Although the CAF represents a major earthquake threat to the nearby City of Murcia, studies on its Quaternary tectonics and seismogenic potential are scarce to date. We present evidence that supports the division of the CAF into two overlapping segments with contrasting tectonic structure, Quaternary activity, and landform control: a SW segment, characterized by a broad fold-and-thrust zone similar to the forebergs defined in the Gobi-Altai region, and a NE segment, characterized by a sharp mountain front controlled by strike-slip tectonics. We attribute the differentiation into these two segments to the stresses associated with topography, which in turn is a consequence of the shortening component, at the middle Pleistocene, after circa 217.4 ka. For the SW segment we infer the occurrence of 9 to 11, M_w 6.7 paleoearthquakes in the last 30.2 kyr, and a slip rate of 0.37 ± 0.08 m/kyr. We date the occurrence of the last surface rupture event after 2750 B.P., and we estimate an average recurrence period of major events of 3.3 ± 0.7 kyr.

1. Introduction

The Eastern Betic Shear Zone (EBSZ) is the main fault system accommodating the convergence between the Eurasian and Nubian plates in Iberia since late Neogene [*Bousquet*, 1979; *De Larouzière et al*., 1988; *Sanz de Galdeano*, 1990; *Silva et al*., 1993]. It shows a characteristic sigmoidal shape extending for more than 450 km from offshore Alboran Sea to NE of Murcia (Figure 1). Along the EBSZ many destructive earthquakes have taken place since historical times proving the seismogenic behavior of the faults that form the shear zone. From southwest to northeast, the EBSZ is formed by the following main faults: Carboneras, Palomares, Alhama de Murcia, Carrascoy, and Bajo Segura [*Instituto Geológico y Minero de España (IGME)*, 2012].

The Quaternary activity of the faults that form the EBSZ has been noticed and studied since the end of the 1970s decade [e.g., *Bousquet*, 1979; *Sanz de Galdeano*, 1983; *Boccaletti et al*., 1987; *Montenat et al*., 1987; *Vegas et al*., 1987; *Masana et al*., 2010; *Buontempo and Wuestefeld*, 2013]. Furthermore, most of these faults have been also studied from a paleoseismological point of view: Carboneras [e.g., *Bell et al*., 1997; *Moreno et al*., 2008; *Moreno*, 2010], Alhama de Murcia [e.g., *Hernández-Enrile and Martínez-Díaz*, 2001; *Ortuño et al*., 2012, *Martínez-Díaz et al*., 2012a], and Bajo Segura [e.g., *Alfaro*, 1995; *García-Mayordomo and Martínez-Díaz*, 2006; *Alfaro et al*., 2012]. The results of these studies have confirmed the capability of these faults for producing large ($M_w > 6.0$), morphogenic earthquakes with an average recurrence of a few thousands of years [*García-Mayordomo et al*., 2012]. Recently, the occurrence of the so-called Lorca earthquake $M_w = 5.1$ (10/05/2011), attributed to the Alhama de Murcia Fault (AMF) [*Martínez-Díaz et al*., 2011, 2012a, 2012b], has demonstrated the threat that smaller, nonmorphogenic earthquakes poses to populations settled on top or very close to active faults in the Betics.

Contrastingly, very little literature has been produced in relation to the Carrascoy Fault Quaternary activity [*Silva*, 1994; *Sanz de Galdeano et al*., 1998; *Leyva et al*., 2010] and its seismogenic potential [*Amores et al*., 2001;

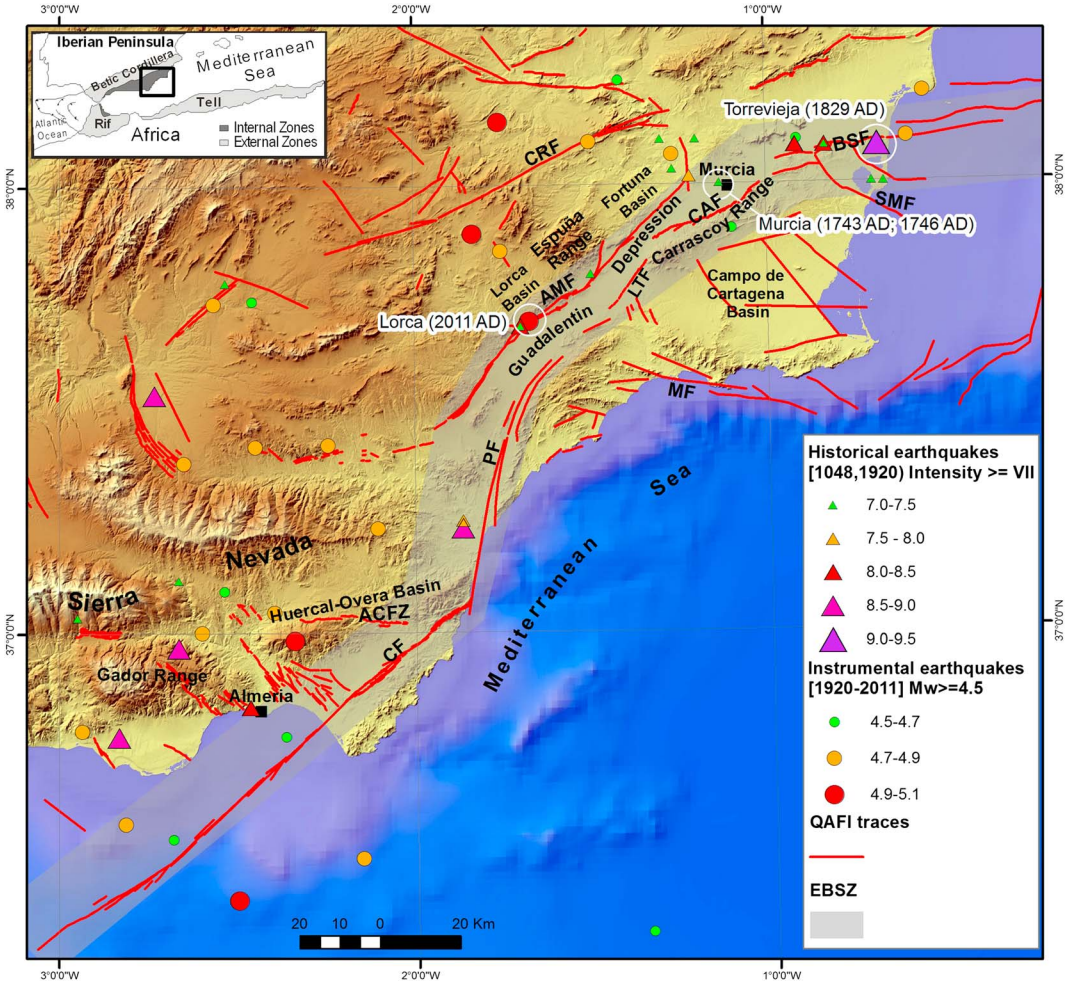

Figure 1. Geological setting of the study area (ED50/UTM Zone 30°N Projection). EBSZ: Eastern Betic Shear Zone (gray shaded); BSF: Bajo Segura Fault; SMF: San Miguel de Salinas Fault; CAF: Carrascoy Fault; LTF: Los Tollos Fault; AMF: Alhama de Murcia Fault; PF: Palomares Fault; CF: Carboneras Fault; CRF: Crevillente Fault; MF: Las Moreras Fault; and ACFZ: Alpujarras Corridor Fault Zone. Fault traces are from an updated version of QAFI database [*IGME*, 2012; *García-Mayordomo et al*., 2012]. Earthquake data corresponds to a declustered version of the Spanish national seismic catalog [*IGN-UPM*, 2013]. The white circles show the identification of major earthquakes cited in the text.

García-Mayordomo and Álvarez-Gómez, 2006]. Furthermore, the cartographic interpretation of the fault is confusing, as in different publications it has been interpreted either as a reverse or left-lateral strike-slip fault, and even as a normal fault [*Silva*, 1994; *Amores et al*., 2002; *Calmel-Avila et al*., 2009; *Leyva et al*., 2010; *Jerez et al*., 2015]. The Carrascoy Fault is a major threat to the city of Murcia, as different seismic hazard assessments in the Region of Murcia have pointed out [*Dirección General de Protección Civil* (*DGPC*), *Civil Protection Special Plan for Seismic Risk at the Region of Murcia* (*SISMIMUR*), 2006; *García-Mayordomo et al*., 2007; *Gaspar-Escribano et al*., 2008] and so its recent tectonics and paleoseismology need to be studied in depth.

In this work we present a new interpretation of the recent tectonics of the Carrascoy Fault based on detailed geological and geomorphological mapping of the Quaternary fault trace carried out from aerial photographs, LIDAR digital elevation model analysis, previous mapping [*Leyva et al*., 2010; *Marín-Lechado et al*., 2011; *Jerez et al*., 2015], field work, and trenching. We present a new model for the segmentation of the fault zone, and its evolution from Pliocene to Quaternary times. A sensible change of trend and kinematic of the Carrascoy Fault is detected. We discussed different reasons that can explain this evolution. Additionally, we bracket the time occurrence of the latest morphogenic earthquakes in the Carrascoy Fault SW segment and estimate their magnitude and average recurrence period.

2. Geological and Geodynamic Setting

2.1. Geological Setting of the Eastern Betics Shear Zone

The Eastern Betics Shear Zone (EBSZ) is the longest fault system of the Betic Cordillera. Some authors have even proposed its connection to the Rif Ranges of northern Africa along the faults of Nekor, naming it the Trans Alboran Shear Zone [*Frizon de Lamotte et al*., 1980; *De Larouzière et al*., 1988]. The EBSZ crosses the easternmost Internal Zones of the Betic Cordillera in a general NE-SW sigmoid shaped trend (Figure 1).

The Betic Cordillera constitutes the northern arm of the Rif-Betic alpine orogenic belt that resulted from the Late Cretaceous-Cenozoic collision between the Nubian and Eurasian plates. The Internal Zones, also referred as the Alboran Domain [*Balanyá and García-Dueñas*, 1987], consist of a stack of tectometamorphic complexes (Nevado-Filabride, Alpujarride, and Malaguide) formed of Paleozoic, Mesozoic, and Tertiary rocks, which occurred mainly by subduction and continental collision processes during the Paleogene [*Egeler and Simon*, 1969; *Azañón et al*., 1997]. The thrust contacts between these major complexes were later reactivated as low-angle normal faults under a regional extensional regime [*Galindo-Zaldívar et al*., 1989; *Aldaya et al*., 1991; *García-Dueñas et al*., 1992; *Jabaloy et al*., 1993; *Azañón et al*., 1998] related to the opening of the South-Balearic basin and coeval with the main westward movement of the Alboran Domain [e.g., *Sanz de Galdeano*, 1990; *Azañón and Crespo-Blanc*, 2000], which lasted at least up to Serravalian times. During the Tortonian an intense magmatic activity took place correlative to the formation of sedimentary basins on both sides of the belt [*Montenat et al*., 1987].

At the end of the Messinian, or beginning of the Pliocene, a rotation of the regional shortening direction to the NNW-SSE [*Ott D'Estevou and Montenat*, 1985] resulted in a tectonic inversion of the Neogene basins and the generation of new sedimentary depressions in areas that were previously uplifted [*Montenat et al*., 1987; *De Larouzière et al*., 1987]. The recent GPS measurements from the CuaTeNeo network in the eastern Betics show a regional shortening direction similar to the present NW-SE convergence trend between the Eurasian and Nubian plates [*Khazaradze et al*., 2008; *Echeverria et al*., 2011].

2.2. Significance of the Carrascoy Fault in the Eastern Betics Shear Zone Context

The Carrascoy Fault represents a major tectonic change in the EBSZ structure and so on the accommodation of the convergence between Nubia and Eurasian plates onshore Iberia. It is estimated that about a third of the 4–6 mm/yr NW-SE convergence between the plates takes place on Iberia onshore [*Argus et al*., 2011; *Serpelloni et al*., 2007]. The Alhama de Murcia fault (85 km long) has being pointed out as one of the major accommodating structures [*Masana et al*., 2004] (Figure 1). However, the Quaternary activity of the Alhama de Murcia fault decreases significantly toward its NE extension. Along the last 25 km stretch of the fault, known as the Alhama-Alcantarilla segment, there is no evidence of deformation younger than Middle Pleistocene and there is a progressive decrease of the geomorphic expression of the fault itself [*Silva*, 1994; *Silva et al*., 2003; *Martínez-Díaz et al*., 2012a]. Contrastingly, ~6 km to the south of the Alhama-Alcantarilla segment the Carrascoy Range emerges (1063 m) and extends to the NE for ~35 km. This prominent mountain range is controlled by the Carrascoy Fault system (see section 3) which takes over the accommodation of the convergence from the Alhama de Murcia fault toward the NE [*Martínez-Díaz et al*., 2012a]. The EBSZ thus experiences a significant modification in this sector of the Betic Range, as it changes from a general NE-SW trend NW dipping structure (Alhama de Murcia Fault) to an ENE-WSW trend SE dipping one (Carrascoy Fault). The connection between the Alhama de Murcia and Carrascoy faults is still poorly understood. Further to the NE, the Carrascoy Fault connects with the E-W Bajo Segura fold-and-thrust zone that extends offshore into the Mediterranean. This is a wide deformation area in which long NW-SE transfer faults are also active (e.g., San Miguel de Salinas and Torrevieja faults) [*Alfaro et al*., 2012]. Offshore studies have shown that the Bajo Segura fold-and-thrust zone widens and attenuates from onshore [*Perea et al*., 2012], suggesting the distribution of the plate convergence in a wider area and so the termination of the EBSZ as a major accommodating single structure.

The Carrascoy Fault Zone presents a lesser seismic activity compared to the neighboring Alhama de Murcia and Bajo Segura faults (Figure 1). Instrumental and historical seismicity occurs preferentially along the most active segments of the Alhama de Murcia (Lorca-Totana and Totana-Alhama segments) and particularly on the Bajo Segura fold-and-thrust zone, where one of the most destructive events ever recorded in Spain took place as recent as 1829 A.D.: the so-called Torrevieja earthquake (IEMS = IX–X, $M_w \approx 6.6$ [*Instituto Geográfico*

Nacional-Universidad Politécnica de Madrid (IGN-UPM), 2013]). Along the Carrascoy Fault Zone and to the south, seismicity is scarce, standing out only four earthquakes recorded between 1931 and 1952, felt with intensities V to VI ($M_w \approx 4.3–4.5$). However, a cluster of earthquakes occurs a few kilometers to the north of the Carrascoy fault, located at the City of Murcia. Practically, all these events correspond to historical earthquakes that took place between 1601 and 1930; the most important ones occurred in 09 March 1743 ($M_w \approx 5.4$) and 15 August 1746 ($M_w \approx 5.1$), felt at Murcia City with intensities VII and VI–VII. The epicenters of these events have been placed in Murcia town, and the most likely causative fault could be any blind fault under the Guadalentin Depression, as if the earthquakes were produced by the Carrascoy Fault there would have been damage reports from the villages settled on the fault trace at the foot of the mountain range. Contrastingly, along the Alhama de Murcia fault more than 10 destructive earthquakes have taken place since 1579, particularly affecting the town of Lorca, reaching intensities up to VIII, being the latest damaging one the 2011 Lorca event ($M_w = 5.1$). In the Bajo Segura fault zone the record of damaging events is even larger, six of them reaching intensity VIII, including the aforementioned 1829 Torrevieja event. Albeit, the scarceness of seismic activity along the Carrascoy fault, its tectonic activity (see section 5.3) is comparable to both the Alhama de Murcia and Bajo Segura faults, suggesting that the Carrascoy Fault may be under an interseismic period of strain accumulation.

3. The Carrascoy Fault System

The Carrascoy Fault system runs NE-SW for about 33 km, constituting the southeastern edge of the northern Guadalentin Depression as well as the northern front of the Carrascoy and Cresta del Gallo ranges [*Silva*, 1994] (Figure 2). At its northeast tip, the trend of the Carrascoy Fault changes to ENE-WSW, connecting to the Bajo Segura Fault, a fold-and-thrust system active since the Pliocene [*Alfaro*, 1995; *Alfaro et al*., 2012]. To the southwest, the Carrascoy Fault is replaced by the Los Tollos Fault, whose Holocene activity and left-lateral reverse kinematics have been recently described [*Insua-Arévalo et al*., 2015].

The Guadalentin Depression is a long morphostructural corridor that is located inside the main displacement zone of the EBSZ (Figure 2a). In the study area, the Guadalentín Depression is bounded to the northwest by the Alhama de Murcia Fault and to the southeast by the Carrascoy Fault, and it is filled up by Pliocene and Quaternary sediments. The Pliocene filling is mainly composed by transitional marine to continental deposits recording the retreat of the sea that began at the upper Messinian and lasted until the early Pleistocene. The Quaternary filling is represented by the accumulation of several generations of alluvial fans that show first-order progressive unconformities evidencing the synchronic activity of the Carrascoy and Alhama de Murcia faults, which control the bounding mountain fronts during the Middle and Upper Pleistocene [*Silva et al*., 1992a, 1992b]. During the Holocene, parts of the Guadalentin Depression became endorheic until approximately 2.5 ka, when a period of fluvial dissection started and lasts to the present [*Silva et al*., 2008; *Calmel-Avila*, 2002].

The Carrascoy Range constitutes the southeastern edge of the northern Guadalentin Depression. This mountain range (1063 m above sea level (asl)) is composed by metamorphic rocks of the Alpujarride and Malaguide Complexes (also known as Alboran Domain). The Carrascoy mountain range can be divided in two distinct sectors according to its morphology and different sedimentary units associated to the range front (Figures 2a and 2b). The NE sector (known as Cresta del Gallo Range) shows a uniform and flat summit line (Figure 2c), and it is composed mainly by metamorphic rocks of the Alborán Domain that form a sharp mountain front that conspicuously bounds the Guadalentin Depression.

The SW sector (Carrascoy Range in a strict sense) shows a summit line increasingly higher to the SW, reaching 1063 m and then abruptly dropping for 800 m to the flat plains of the central part of the Guadalentin Depression (Figure 2c). The mountain front at this sector can be also divided in two distinct parts (Figure 3): a southern, higher front, which controls the contact between the metamorphic rocks of the Alboran Domain and late Neogene marine sediments as well as continental Plio-Quaternary deposits, and a northern, lower front that puts in contact the continental Plio-Quaternary deposits with the most recent Quaternary alluvial fans, corresponding to the current, active mountain front. These Plio-Quaternary deposits are remains of older alluvial fans coming from the higher parts of the Carrascoy Range and are named locally either as the Rambla Conglomerate Formation [*Silva*, 1994] or the Red Unit (*Jerez et al*., 2015). Hereinafter, we refer to them as the Red Unit.

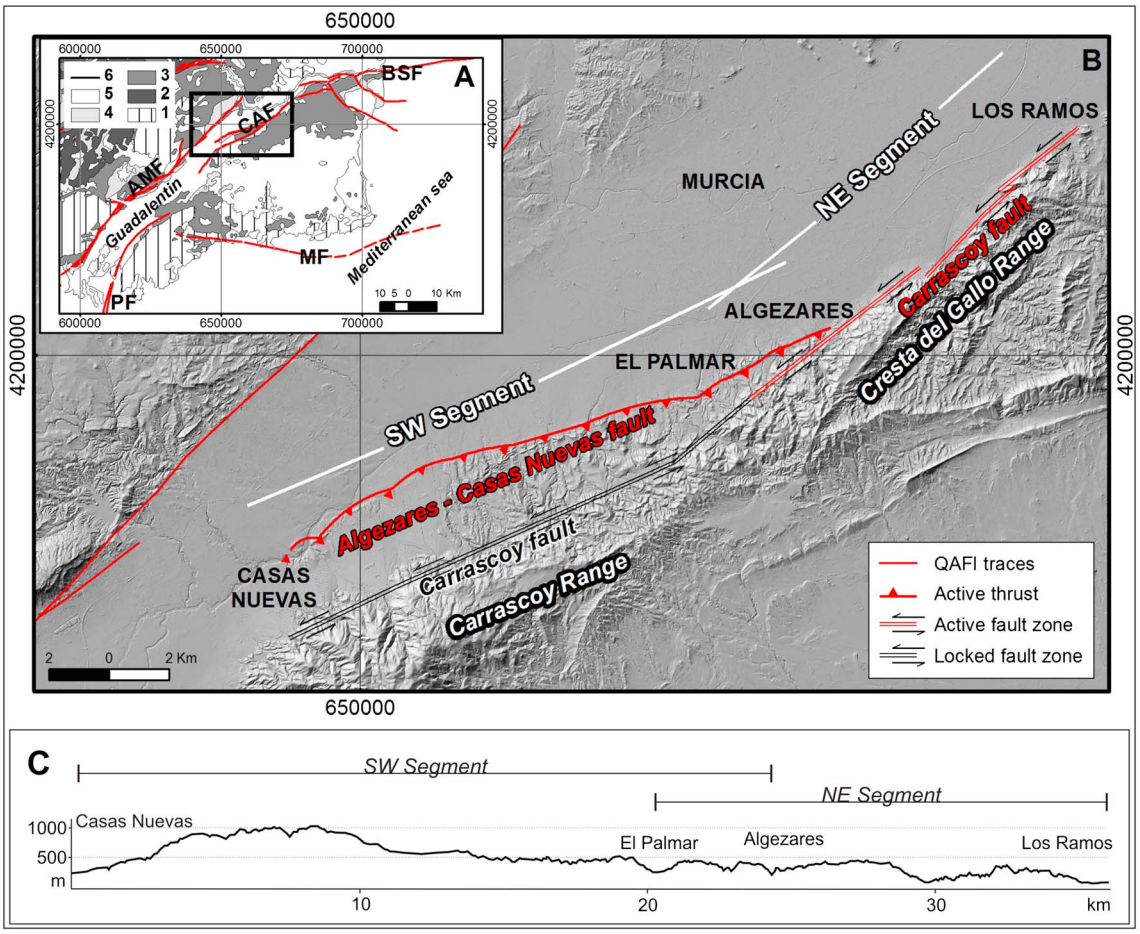

Figure 2. (a) Local tectonic frame of the Carrascoy Fault (CAF) (ED50/UTM Zone 30°N Projection). 1: Internal Zones; 2: Subbetic; 3: Neogene; 4: Plio-Pleistocene; 5: Quaternary; 6: BSF: Bajo Segura Fault; AMF: Alhama de Murcia Fault; MF: Mazarrón Fault; and PF: Palomares Fault. (b) Proposed new segmentation of the CAF over a digital elevation model (ETRS1989/UTM Zone 30°N Projection). (c) Topographic profile along the Carrascoy and Cresta del Gallo ranges.

3.1. Segmentation of the Carrascoy Fault System

Based on regional differences on the structural pattern and kinematics of the Carrascoy Fault, *Silva* [1994] proposed the division of the fault in three segments: a southern one called Casas Nuevas-El Palmar, a central one called El Palmar-La Zeneta, and a northern one called Jacarilla-Guardamar. In this section we present new evidence that refines this general segmentation for the first two segments (Figure 2b), as the latter is nowadays known as the Bajo Segura Fault.

The Carrascoy Fault controls both the NE and SW sectors of the Carrascoy Range described in the preceding section. The fault is formed by two overlapped segments (Figure 2b). The NE segment is 16 km long and stretches from Los Ramos to El Palmar villages in a N050°E trend. It is formed by a narrow fault zone that *Silva* [1994], *Sanz de Galdeano et al.* [1998], and *Leyva et al.* [2010] called "Nor-Carrascoy fault" because controls the conspicuous and sharp mountain front of the northern edge of the Carrascoy Range. However, in order to avoid misunderstandings relative to name and its geographical position in the segment SW, we have decided to call it "Carrascoy fault." This fault has been described by previous authors as a left-lateral strike-slip subvertical fault dipping southeastward.

The SW segment is 23 km long and comprises a much broader fault zone that stretches from Algezares village to Casas Nuevas district, close to the Guadalentin River. This wide fault zone is bounded by two main faults, the Carrascoy Fault extension toward the southwest and the hereinafter referred as Algezares-Casas Nuevas Fault. The later diverges from the former in the Algezares area and controls a lower mountain front bounding the Guadalentin Depression (Figure 2b). The Carrascoy Fault ends abruptly at the southwest termination of the Carrascoy Range, while the Algezares-Casas Nuevas Fault ends accommodated in a broad antiform in

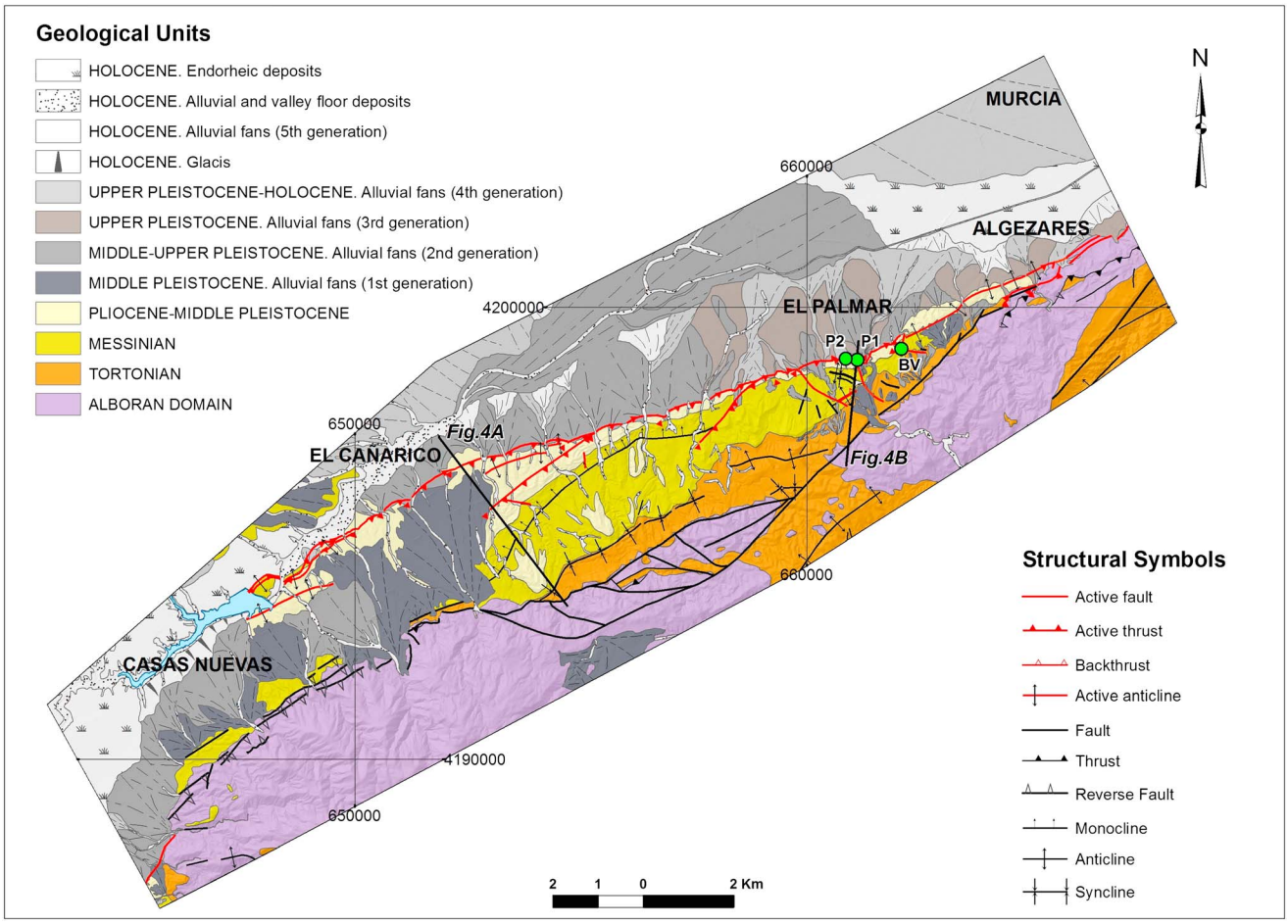

Figure 3. Geological map of the study area over a digital elevation model (ED50/UTM Zone 30°N Projection). The location of the trenches is displayed: P1: Palmar-1; P2: Palmar-2; and BV: Buenavista road cut. El Cañarico (Figure 4a) and El Palmar (Figure 4b) geological cross sections are also displayed.

the Casas Nuevas area. The nature of the Algezares-Casas Nuevas Fault is unclear, as some authors have considered it either as a left-lateral strike-slip fault, as a blind reverse fault dipping to the south or even as a normal fault dipping to the north [*Silva*, 1994; *Amores et al*., 2002; *Calmel-Avila et al*., 2009; *Leyva et al*., 2010; *Jerez et al*., 2015].

3.2. The SW Segment: Carrascoy and Algezares-Casas Nuevas Faults

The Carrascoy Fault (Figure 2b and 3) controls the most important reliefs of the Carrascoy Range. This fault zone shows a N055–065°E trend and deforms both the metamorphic rocks of the Alboran Domain and Late Neogene marine deposits (Figure 3). The Carrascoy Fault is a left-lateral strike-slip fault with a reverse component. The tight syncline formed in the Tortonian rocks located on the downthrown block, running parallel to the fault, shows a clear reverse component.

The area in between the Carrascoy and Algezares-Casas Nuevas faults is an area of a moderate topography compared to the Carrascoy Range. The Algezares-Casas Nuevas fault is arranged in a left-stepping en echelon pattern increasing the width of the fault zone toward the southwest from the Algezares village. In this area, blind reverse faults and folds are developed both in late Neogene marine deposits as well as in Plio-Quaternary continental alluvial fans that form the Red Unit. A clear example is the kink fold in El Cañarico village (Figure 4a).

The area in between the Carrascoy and Algezares-Casas Nuevas faults is interpreted as a fold-and-thrust zone developed on the foreland area of the Carrascoy fault. Both faults should connect at depth, being Algezares-Casas Nuevas the youngest basinward strand, and responsible of the current active mountain front (Figures 4a and 4b).

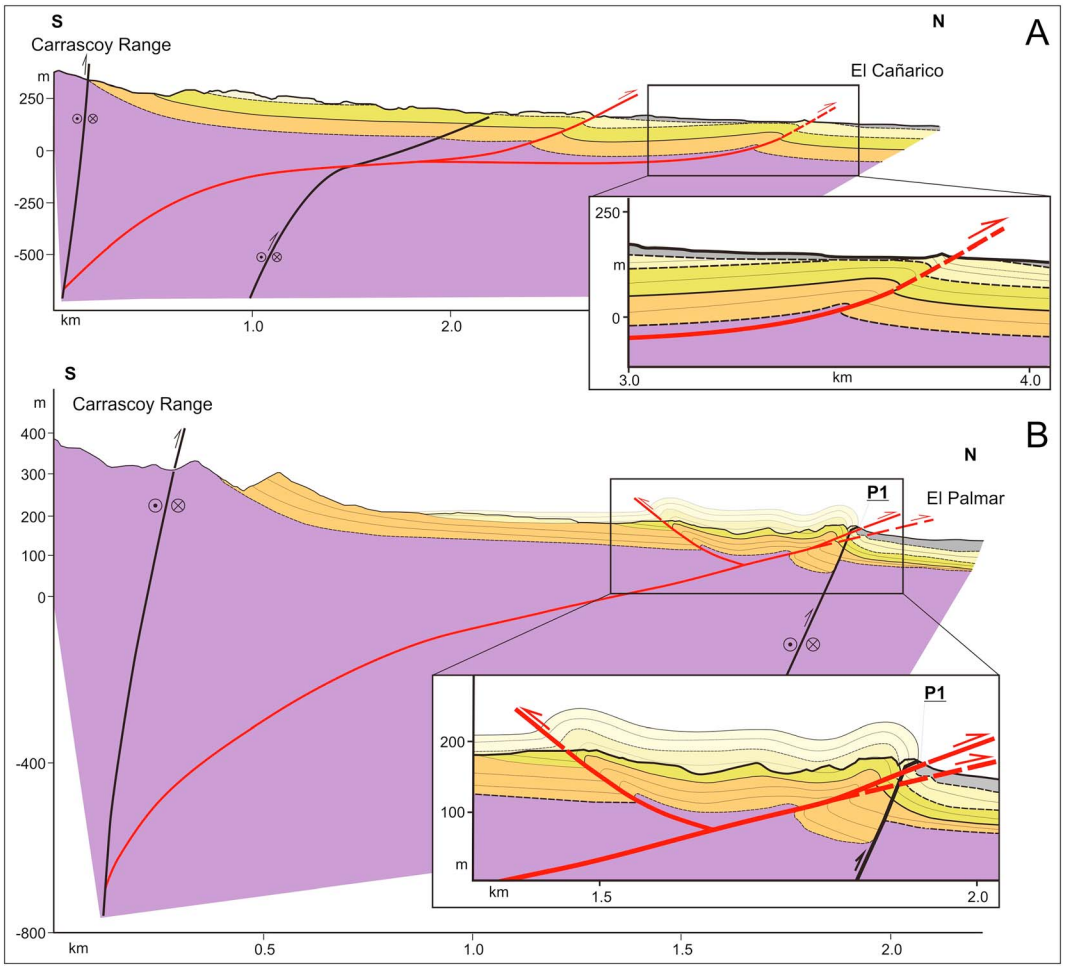

Figure 4. (a) Geological cross section from Carrascoy Range (South) to El Cañarico district (North). (b) Geological cross section from Carrascoy Range (south) to the Palmar-1 trench (north). Color caption is common to Figure 3.

The fold-and-thrust zone broadens toward the southwest while to the northeast it eventually disappears at Algezares village, where the Carrascoy and Algezares-Casas Nuevas faults merge. The outcrop extension of Late Neogene and Red Unit deposits shows the same tendency, their surface expression disappearing at Algezares village (Figure 3). Regarding to the Quaternary alluvial fans arrangement, at the southwest part, the morphology of the fans belonging to the first generation (middle Pleistocene) is still preserved from erosion, while to the northeast only few remnants of these fans are preserved. Furthermore, at the southwest part, the alluvial fans of the second generation (middle–upper Pleistocene) spread out from the Carrascoy Range and onlap the backlimb of the Algezares-Casas Nuevas fault propagation fold, which represents the current active mountain front; on the contrary, to the northeast, these alluvial fans spread directly away from the current mountain front.

The age of the distinct generations of alluvial fans defined in this paper is based on previous work [*Silva*, 1994; *Leyva et al*., 2010; *Jerez et al*., 2015], and refined by our geomorphologic analysis and numerical dating.

4. Recent Tectonics and Paleoearthquakes at the SW Segment of the Carrascoy Fault

The structural interpretation of the SW segment of the Carrascoy Fault described above is supported by the observations carried out at two trenches dug in El Palmar area (Palmar-1 and Palmar-2, Figures 5 and 6) and at a road cut exposure (Buenavista, Figure 7). The Palmar-1 trench was set at the foot of the current mountain front formed by the folding of the Red Unit sediments and the Palmar-2 at the mouth of a gully dissecting the

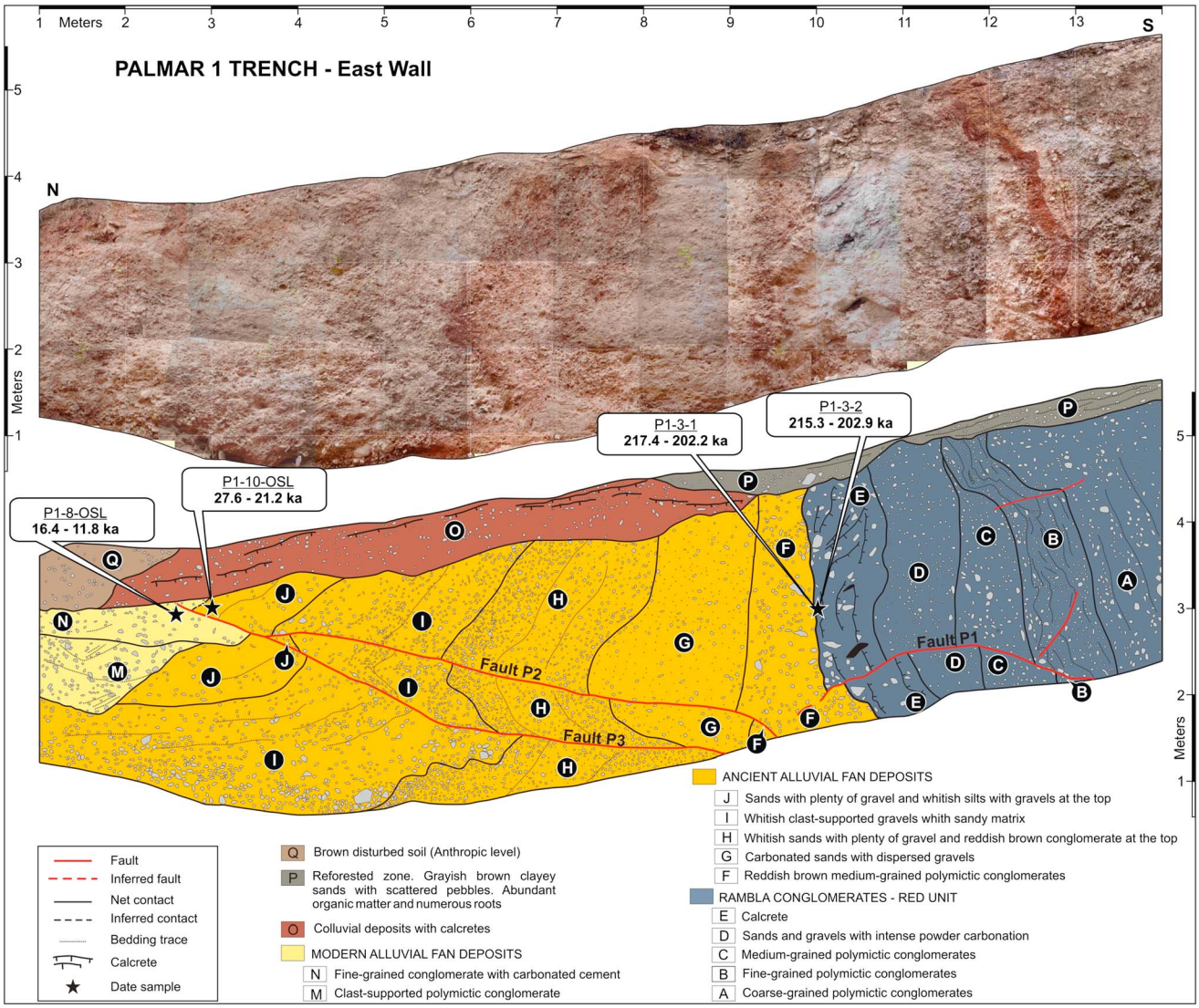

Figure 5. Photographs and log of the eastern wall of the Palmar-1 trench.

mountain front. Carrying out paleoseismological studies in reverse blind faults is very challenging, particularly when faults are slow and, therefore, recent tectonic landforms are easily obliterated, especially when the territory has been subjected to a very intense anthropogenic modification, which is the general situation in Murcia Region.

4.1. Palmar-1 Trench

Palmar-1 trench brought to light a set of south dipping low-angle reverse faults affecting Red Unit sediments and younger alluvial fan deposits (Figure 5). The Red Unit outcrops at the southern part of the trench showing vertical bedding and consists of red conglomerates and sandstones with clay matrix (units A to E, see legend in Figure 5). The top of the Red Unit is characterized by a thick, very well developed calcrete (unit E). It consists of a densely cemented hardpan horizon (20 to 40 cm thick) overlain by a thin, 2 cm thick, laminar crust. This calcrete was the object of a detailed study in order to constraint the latest moment at which the calcrete was developed [*Herrero et al*., 2014]. Unit E is overlaid by a first alluvial fan sequence (Aluvial I: units F to J). It is constituted by tabular conglomeratic bodies dipping vertically (unit F) and then increasingly less northward (30°, unit J). A gradual increase of the thickness of each of the layers northward is also observed. A second alluvial sequence (Alluvial II) is defined by units M to N. It consists of gravels, sands, and silts with channel morphologies that rest unconformably on Alluvial I units (I and J). The top part of the trench is blurred by

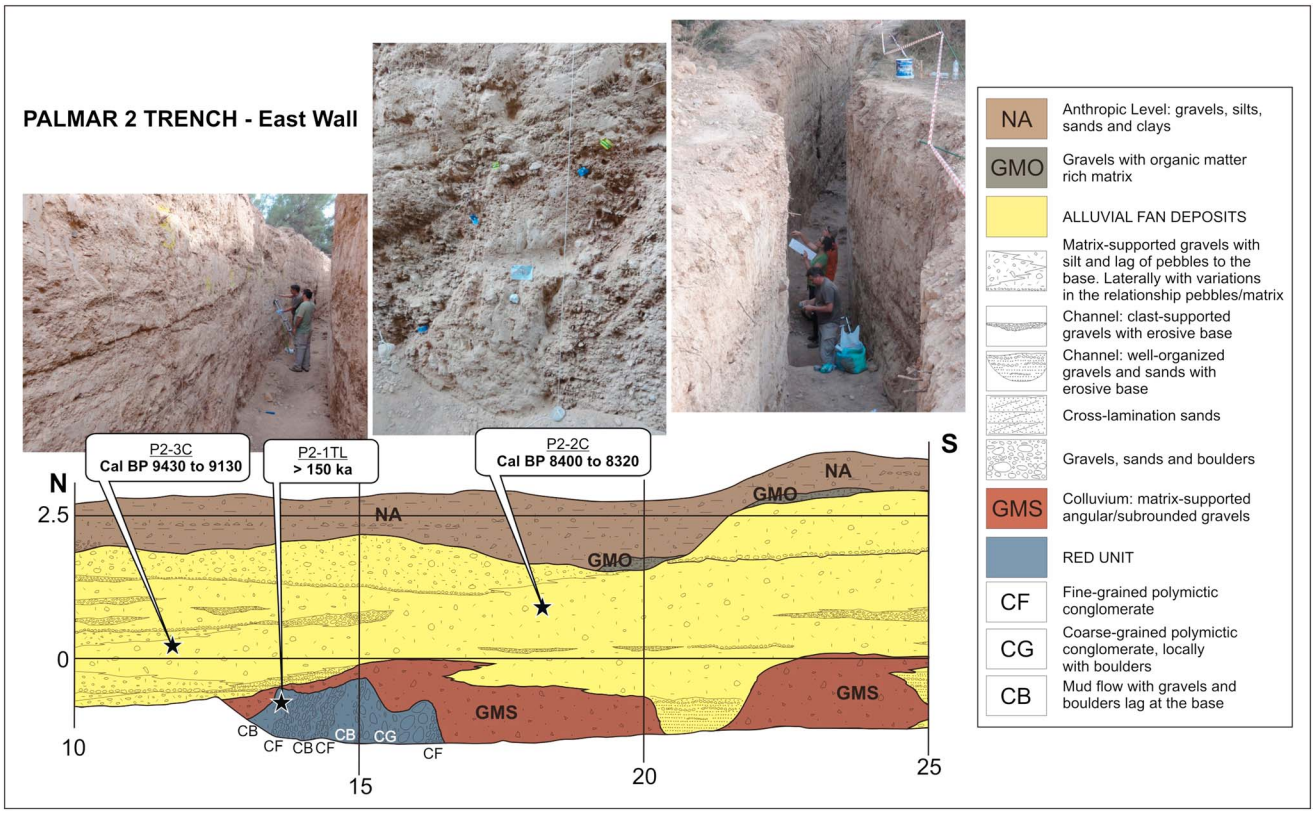

Figure 6. Photographs and log of the eastern wall of the Palmar-2 trench.

an intense carbonatic edaphization and it also shows an intense anthropization (units O and Q). At the northern part of the trench an anthropic horizon related to historical pine tree reforestation was also identified (unit P).

The set of low-angle reverse faults show a N128°E average strike and 20° dip to the south (Figure 5). The apparent obliquity of the mapped trend of the fault is due to the location of the trench at a local curvature of the fault plane. It consists of two single faults (Faults P2 and P3) that merge at the floor of the trench. The striae found on the fault planes (75–80° rake) indicate an almost pure reverse movement. Detailed measurements of the fault offsets showed that they correspond to just a single movement, with a net displacement of approximately 68 cm. Considering also the ductile deformation from the dragging of the markers, the total net slip reaches approximately 1.30 ± 0.1 m. The faults clearly cut across both Aluvial I and II sequences and reach to the surface, although the intense edaphization and anthropization of the topmost unit (O) precludes the observation of obvious offsets. Finally, inside the Red Unit a curved-shaped fault is shown (Fault P1, Figure 5). This fault offsets and drags the bedding in Red Unit deposits, also affecting the base of the first body of Alluvial I sequence (unit F). The interpretation of this fault is presented in the discussion section of this paper.

The laminar crust developed on top of the calcrete deposit (unit E) was carefully sampled and dated using U-series disequilibrium techniques. Two samples were analyzed (P1-3-1 and P1-3-2) providing a consistent age of 217.4–202.2 and 215.3–202.9 ka, respectively (Hoffmann, D., Report U-series analyses, MC-ICPMS U-series Laboratory, Geochronology Programme, CENIEH, Burgos, Spain, 2013) (Table 1). Additionally, silt levels in units J (Alluvial I, P1-10-OSL) and N (Alluvial II, P1-8-OSL) were sampled for OSL dating. The analyses showed that the samples were highly affected by incomplete bleaching and, therefore, a minimum age model was chosen to estimate the true burial dose. The Internal-External Consistency Criterion (IEU) [*Thomsen et al.*, 2003, 2007] was chosen, as it proved to be appropriate for sediments from the same area [*Medialdea et al.*, 2014]. The results provided ages of 16.4–11.8 and 27.6–21.2 ka for P1-8-OSL and P1-10-OSL samples, respectively (Table 1).

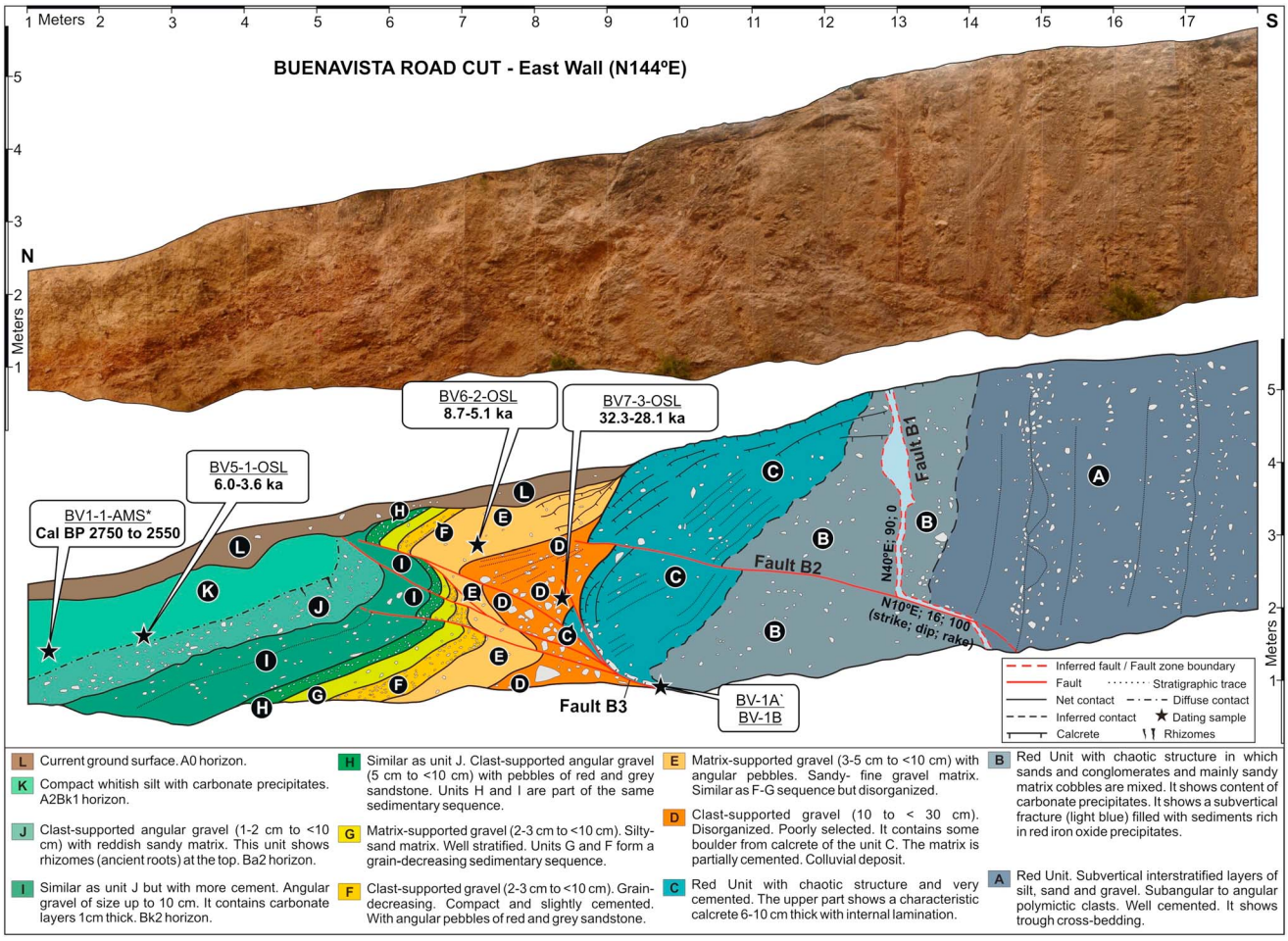

Figure 7. Photograph and log of the Buenavista road cut.

4.2. Palmar-2 Trench

The Palmar-2 trench was dug parallel to a broad flat valley coming out of the mountain front and forming the largest of the alluvial fans that coalesce on the border with the Guadalentin Depression. The plan for the trench was set after the interpretation of an electrical tomography profile performed on the site for this purpose [*Ibarra et al.*, 2012]. The calcrete layer developed on top the Red Unit in Palmar-1 trench (Unit E in Figure 5) worked as a resistive layer and was used as a guide to estimate approximately the location of the fault.

The Palmar-2 trench shows a sequence of alluvial sands and silt layers unconformably overlying a small outcrop of Red Unit deposits located in the central part of the trench at a depth of 3 m (Figure 6). Two charcoal samples (P2-2C and P2-3C) were found embedded in silt layers within the alluvial deposits. The samples were analyzed by accelerator mass spectrometry (AMS) radiocarbon and provided ages of Cal B.P. 8400 to 8320 and Cal B.P. 9430 to 9130, respectively, for 2 sigma calibrated results (Table 1) (Tamers, M.A. and D.G. Hood, Report of radiocarbon dating analyses, Beta Analytic Inc., Miami, Florida, USA, 2012). In the Red Unit, an additional sample was taken from a silty layer (P2-1TL). This sample was analyzed by the thermoluminescence (TL) dating technique, and its age was found beyond the accuracy of the method, being at least older than 150 ka (Debenham, N., Thermoluminescence dating of sediments from the Betic Cordillera, Murcia, Quaternary TL Surveys, Nottingham, UK, 2013).

In spite of the 4 m depth and 35 m length of the trench, the excavation did not expose the fault. However, the electric profiles performed previously suggested the location of the fault in an area that coincides with the section where the small outcrop of Red Unit appeared at the bottom of the trench. According to the electric profiles the fault plane should be located at around 10 m depth at this section [*Ibarra et al.*, 2012].

Table 1. Summary of Results for U-Series Analyses[a], OSL Age Calculation, and AMS-Radiocarbon Data[b]

Site	Sample ID	230Th/238U	234U/238U	U-Th Age (ka)
Palmar-1	P1-3-1	1.118 ± 0.007	1.249 ± 0.012	209.8 ± 7.6
Palmar-1	P1-3-2	1.158 ± 0.007	1.288 ± 0.010	209.1 ± 6.2
Buenavista	BV-1A′	2.618 ± 0.021	1.935 ± 0.012	nd
Buenavista	BV-1B	2.668 ± 0.023	1.954 ± 0.013	nd
Site	Sample ID (Depth/Water)	Dose (Gy)	Rate (Gy/ka)	OSL Age (ka)
Palmar-1	P1-8-OSL (80 cm/17%)	16.4 ± 2.5	1.16 ± 0.05	14.1 ± 2.3
Palmar-1	P1-10-OSL (70 cm/17%)	34.0 ± 4.2	1.39 ± 0.06	24.4 ± 3.2
Buenavista	BV5-1-OSL (97 cm/4%)	10.5 ± 2.6	2.20 ± 0.10	4.8 ± 1.2
Buenavista	BV6-2-OSL (78 cm/13%)	11.7 ± 3.0	1.71 ± 0.08	6.9 ± 1.8
Buenavista	BV7-3-OSL (180 cm/4%)	64.0 ± 3.1	2.07 ± 0.10	30.2 ± 2.1
Site	Sample ID	Material/Pretreatment	Conventional Radiocarbon Age	2 Sigma Calibrated Result
Palmar-2	P2-2C	charred material: acid/alkali/acid	7530 ± 40 B.P.	Cal B.P. 8400 to 8320
Palmar-2	P2-3C	charred material: acid/alkali/acid	8290 ± 40 B.P.	Cal B.P. 9430 to 9130
Buenavista	BV1-1-AMS	organic sediment: acid washes	2560 ± 30 B.P.	Cal B.P. 2750 to 2700 Cal B.P. 2630 to 2620 Cal B.P. 2560 to 2550

[a]Activity ratios and age are for corrected values. Samples BV-1A′ and BV-1B show 230Th/238U activity ratios that exceed the possible range of natural activity ratio development, indicating U leaching and open system behavior.
[b]INTCAL09 Calibration [*Heaton et al.*, 2009; *Reimer et al.*, 2009; *Stuiver and Braziunas*, 1993; *Oeschger et al.*,1975].

4.3. Buenavista Road Cut

Close to the Buenavista residential area, south of El Palmar village, there is a private road leading to the sierra which shows an excellent outcrop where it crosses the current mountain front. The road cut (Figure 7) shows, from south to north, Red Unit deposits vertically arranged (units A and B) with a very thick calcrete layer developed on top (unit C) followed by a colluvial deposit of reworked gravels and blocks showing a chaotic structure containing fragments of the underlying calcrete (unit D). The upper part of Unit D shows a set of calcrete laminations with an increase in dip to the south. Unit E overlies Unit D, presenting a similar chaotic structure but with a much thinner grain size. On top of this unit occurs an alluvial sequence of two tabular bodies composed of gravels showing a decrease in grain size (units F and G), followed by a second alluvial sequence composed of clast-supported gravels (units H to J). The top of this last sequence is formed by a calcified silt deposit (unit K). A current organic soil horizon is identified at the top of the trench (unit L).

Three different soil generations can be inferred from units I to L. Unit I shows a very intense calcification while the overlying unit J shows a conspicuous accumulation of red clays. We interpreted these two units as a calcic horizon (Bk2) and an argillic horizon (Bt2) of an older soil. The following unit K shows a very important calcification developed in a silty matrix deposit with abundant organic matter, and it is interpreted as a calcic horizon of a younger soil developed on a previous organic horizon (A2Bk1). Finally, the topmost unit of the outcrop, unit L, is the organic horizon developed from the current active soil processes (A0). It is interesting to note the characteristic calcified roots that appear at the contact between units J (Bt2) and K (A2Bk1), which are interpreted as being developed during soil generation 2 and later calcified during soil generation 1.

The calcrete deposit developed on top of the Red Unit (unit C) is visibly folded and shows two N010°E, 16–20°S reverse faults cutting through (Figure 7). The upper fault (Fault B2) can be followed from the southern part of the road talus, cutting through Red Unit deposits and offsetting units C and D. Fault offset seems to attenuate upward, ranging from a maximum of 1.2 m to a minimum of 0.4 m, reflecting attenuation of displacement toward the surface. The lower fault (Fault B3) shows a set of reverse splays that cut through unit C offsetting unit D, and cutting and folding all the alluvial sequence on top (units E to K) until the current soil horizon (unit L), which seals the deformation. A minimum cumulative displacement of 2.2 ± 0.3 m has been estimated, which includes the offset observed on the each fault strand and the folding of the affected units (drag fold). The calcified roots on top of unit J appear clearly tilted, evidencing that this deformation took place after soil generation 1, and previously to the development of the current active soil (unit L). Finally, inside the Red Unit a N040°E,90° fault breccia is observed (Fault B1). Striae found inside the fracture zone have a rake of 0°, clearly evidencing strike-slip kinematics. This fault is offset 1.2 m by the upper reverse fault described above.

The calcrete layer developed on top of the Red Unit (unit C) was sampled for U-Th dating. These samples resulted contaminated and useless for age dating (Table 1). Three other samples were collected for OSL dating in units K, E and D (BV5-1-OSL, BV6-2-OSL, and BV7-3-OSL, respectively) and another one for AMS radiocarbon dating in unit K (BV1-1-AMS) (Table 1). The OSL method provided consistent ages of 32.3–28.1 ka for Unit D and 6.0–3.6 and 8.7–5.1 ka for units K and E, respectively. AMS dating for BV1-1-AMS was performed on organic matter contained in the sediment and provided a 2 sigma calibrated age of B.P. 2750 to 2550 (2 sigma calibrated results: 2750 to 2700 B.P., 2630 to 2620 B.P., and 2560 to 2550 B.P., see original data in Tables S1–S5 captions in the supporting information) (Tamers, M.A. and D.G. Hood, Report of radiocarbon dating analyses, Beta Analytic Inc., Miami, Florida, USA, 2012).

5. Discussion

5.1. On the Segmentation of the Carrascoy Fault Zone

This work adds new evidence to redefine the previous segments proposed by *Silva* [1994] (i.e., Zeneta-El Palmar and El Palmar-Casas Nuevas). Here we define two segments: the NE segment that extends between Los Ramos and El Palmar villages, and the SW segment between Algezares and Casas Nuevas villages (Figure 2b). This segmentation proposed is based on their different tectonic structure, recent kinematics and, consequently, recent landform control, although it exists a well-defined overlapping area between the Algezares and El Palmar villages.

The NE segment is formed primarily by a single fault zone that is the Carrascoy fault, which shows a consistent left-lateral with reverse component kinematics since late Neogene [*Silva*, 1994; *Sanz de Galdeano et al*., 1998; *Leyva et al*., 2010], and controls a conspicuous, sharp N050°E mountain front for 16 km. The summit line of the Carrascoy Range along this segment shows a uniformly constant height not exceeding 500 m asl until northeast of the village of Los Ramos, nearby Zeneta village. Moreover, for most of its length, the mountain front coincides with the contact of Alboran Domain rocks with third and fourth alluvial fans generations (upper Pleistocene and upper Pleistocene–Holocene, respectively).

Conversely, the SW segment comprises a wider fault zone formed by two main strands: the extension of the Carrascoy Fault to SW and the N065°E Algezares-Casas Nuevas fault, which is the youngest, active strand of the segment. This fault is a pure reverse blind fault that controls the current active mountain front along this segment. The Carrascoy Range summit line controlled by the old, currently inactive, and southwestward extension of the Carrascoy Fault shows an increasing altitude from near 500 m asl at the Cresta del Gallo Range (Algezares) to 1063 m asl at the southwestern end of the range, suggesting that there has been a progressive uplift toward the southwest.

We proposed that the development of the Algezares-Casas Nuevas fault, and hence its diversion from the Carrascoy fault, has taken place progressively from Algezares village toward the southwest. Consistently, the outcrop extension of late Neogene and Red Unit sediments steadily increases from Algezares toward the southwest, reflecting the broadening of the fold-and-thrust zone in between both faults. The Carrascoy and Algezares-Casas Nuevas fault strands merge in the area spanning from El Palmar to Algezares villages. In this area the folding associated to the Algezares-Casas Nuevas fault-front is offset by tear faults, suggesting accommodation of the deformation into a narrower space in between both faults. The folding and thrusting of the Red Unit deposits progressively attenuates from El Palmar to Algezares villages, until it disappears under the alluvial fan deposits of third and fourth generation (upper Pleistocene-Holocene). The termination of the thrust deformations is shown at the foot of the hill in Algezares village, where the topography reflects a stepped relief associated with the upthrown and downthrown blocks of the fault, controlling the urban development. From this point to the northeast, the Carrascoy left-lateral strike-slip fault takes over until Los Ramos village, where a dramatic change in the relief morphology trend occurs, from N050°E to N090–100°E, marking the inception of the well-known Bajo Segura blind thrust system.

The Bajo Segura Fault folds and thrusts a continental formation of similar characteristics to those of the Red Unit, known as the Guadalentin Conglomerate Formation [*Montenat*, 1973, 1977; *Soria et al*., 1996]. This is a fluvial formation with an age spanning from Pliocene to Middle Pleistocene [*Goy et al*., 1989; *Bardají et al*., 1995]. We proposed here that the Guadalentin Conglomerate Formation is the lateral equivalent of the Red Unit outcropping in our working area. This is consistent with the age obtained for the calcrete layer

developed on top of the Red Unit at El Palmar area, 217.4–202.2 ka (upper part of the middle Pleistocene). Hence, the recent, strong reverse character of the SW segment is responsible for the outcropping of the Red Unit by uplifting and folding. To the NE, this unit is buried by Quaternary alluvial fans (upper Pleistocene-Holocene) associated to the NE segment appearing again uplifted and folded by the Bajo Segura Fault. The onset of pure reverse kinematics at the SW segment of the Carrascoy Fault Zone can be constrained by the detailed observations achieved at the trenches and described in the following section.

5.2. Recent Tectonics and Paleoseismological Observations

5.2.1. Palmar-1 and Palmar-2 Trenches

The different sedimentary units and tectonic structures observed in the Palmar-1 trench can be interpreted invoking three distinct tectono-sedimentary phases: (1) sedimentation of the Red Unit (Pliocene to middle Pleistocene) synchronic with left-lateral reverse kinematics, (2) sedimentation of the Alluvial I sequence (middle–upper Pleistocene) synchronic with folding, and (3) sedimentation of Alluvial II sequence (upper Pleistocene-Holocene) and the subsequent thrust faulting.

The first phase is inferred by the faults found affecting the Red Unit sediments and the base of the Alluvial I sequence (unit F). These faults show a conspicuous curved shape indicating that they have been folded coevally with the Red Unit in a subsequent phase. Restoration of the Red Unit bedding planes to horizontal shows that these faults would trend N050°E/60°SE and their striae would rake 10–25°W evidencing a left-lateral strike-slip kinematics with a reverse component, similar to the Carrascoy Fault (Fault P1, Figure 5).

The subsequent phase of deformation is constrained by the U-Th analysis of the calcrete developed on top of the Red Unit (unit E, Figure 5), which provided a consistent date of 217.4–202.2 ka (upper part of the middle Pleistocene). The beginning of this second phase of deformation should be younger than the lower limit of this rank (217.4 ka) (C Fault, Figure 8), as Red Unit materials experienced uplifting and folding, feeding new alluvial deposits that recorded syntectonic sedimentation (Alluvial I sequence) (Alg Folding, Figure 8). This is shown both by the decreasing dip and thickening of the Alluvial I sedimentary bodies northward. This deformation records the accommodation of a fault propagation fold, as a result of the summation of multiple seismic events.

The third phase follows with the sedimentation of the Alluvial II sequence (units M and N). At some point after the sedimentation of these units, all the sedimentary record appears faulted by a set of low-angle reverse faults dipping and merging southward (Faults P2 and P3, Figure 5).

This faulting represents a unique, last earthquake recorded in the trench showing the propagation to the surface of the blind thrust responsible for the folding of the Red Unit and the Alluvial I sequence (event Pz, Figure 8). Striae have been found on the fault planes with rakes close to 90°, showing an almost pure reverse kinematics. This last earthquake can be predated by considering the OSL date obtained for the youngest affected unit (Unit N), which provided and age of 16.4–11.8 ka. This paleoearthquake is postdated by the nondeformed sediments that overlie the Red Unit in the Palmar-2 trench—i.e.: Cal B.P. 9430 to 9130 (P2-C3). Hence, the occurrence of the last surface rupture event in this trench took place between 16.4 and 9.4 ka (event Pz, Figure 8).

5.2.2. Buenavista Road Cut

Buenavista road cut interpretation shares similarities and differences to Palmar-1 trench. A major difference regards to the interpretation of the vertical N040°E pure strike-slip fault found inside the Red Unit deposits (Fault B1, Figure 7). Opposite to Palmar-1 trench, here this fault does not appear folded and its subparallel strike to bedding evidences that it was produced after the folding of the Red Unit (Alg Folding, Figure 8). This situation suggests that strike-slip kinematics has continued active at the northern end of the SW segment of the Carrascoy Fault Zone, at least in the Buenavista site, after the onset of the folding, active since circa 217.4 ka, following the interpretation in Palmar-1 trench (C Fault, Figure 8). It seems plausible that the area where both SW and NE segments merge shows overlapping ruptures with characteristic kinematics of each segment, reverse and strike slip, respectively, for the SW and NE segments. The reverse fault identified at the southern part of the outcrop at Buenavista (Fault B2, Figure 7), offsets the N040 strike-slip fault by 1.2 m as well as the colluvial deposit that overlies the folded Red Unit (Unit D, Figure 7). This deposit has an estimated OSL age of 32.3–28.1 ka (BV7-3-OSL, Table 1), while the nonfaulted deposit on top (unit E) provided an OSL age of 8.7–5.1 ka (BV6-2-OSL, Table 1). Hence, the reverse rupture occurred between 32.3 and 5.1 ka (event Bx, Figure 8) while the strike-slip rupture was older (C fault, Figure 8). In addition, the strike-slip faulting

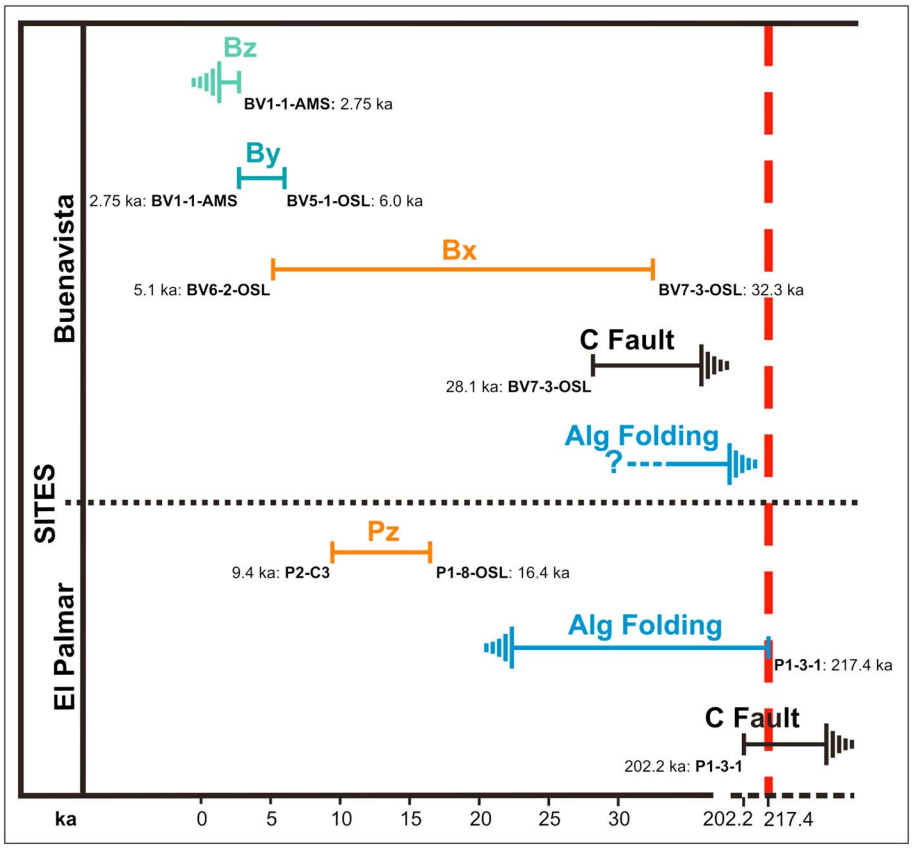

Figure 8. Interpretation of surface rupture events and deformation phases at Palmar and Buenavista sites. Earthquake events are labeled and ordered according to the site (P and B for Palmar trench and Buenavista, respectively). C and Alg stand for Carrascoy and Algezares-Casas Nuevas faults, respectively. The dates and sample names that bracket the events are also shown, see Table 1 for a detailed description. The red line marks the onset of the activity of the Algezares-Casas Nuevas Fault.

took place after the folding of the Red Unit (Alg Folding, Figure 8), when the Algezares-Casas Nuevas fault was already active, suggesting that both kinematics coexisted in this overlapping area.

A similarity between Palmar-1 and Buenavista outcrops is the observation at both sites of syntectonic deposits related to active folding. The Unit D is interpreted as colluvial deposits formed close to the scarp generated by the folding of the calcrete developed on top of the Red Unit (unit C). Unfortunately, we were not able to obtain a U-Th age estimation of this unit as we were in Palmar-1 trench (Table 1). The following alluvial sequences (units E-F-G and H-K) were formerly deposited overlying this scarp, and latter intensively folded and offset by the set of reverse faults identified at the bottom part of the outcrop (Fault B3, Figure 7).

At least two single surface rupture events can be discriminated at Buenavista based on the two distinct reverse faults that affect differently the sedimentary units (events Bz and Bx, Figure 8). The oldest event (event Bx, Figure 8) is related to the reverse fault of the upper part of the outcrop (Fault B2, Figure 7) and its occurrence is bracketed between 32.2 and 5.1 ka, as described above for units D and E, respectively. The youngest event (event Bz, Figure 8) is related to the thrusting and folding of the E to K units (Fault B3, Figure 7). These units show an intense kink like folding producing a net slip of 2.2 ± 0.3 m, which is larger than the accumulated slip on the reverse fault splays suggesting that prior to being offset the units were already folded by an intermediate event (event By, Figure 8). This event would be responsible for the dip of the units (~20°) in the footwall, occurring after of the deposit of the Unit K (6.0–3.6 ka). Radiocarbon AMS dating of the organic matter contained in unit K, corresponding to an A1Bk2 horizon, provided an age of Cal B.P. 2750–2550. Hence, the last surface rupture event at Buenavista took place after 2750 B.P. (event Bz, Figure 8).

It is interesting to note that the youngest event in Buenavista (event Bz, after 2750 B.P.) is not registered in Palmar-1 trench (Figure 8). Moreover, according to Palmar-2 trench radiocarbon ages of nondeformed sediments, no rupturing events have taken place at least since Cal B.P. 9130. This situation can be explained either by assuming that the fault producing the youngest event in Buenavista did not rupture at El Palmar area, or simply considering that this event is missed at Palmar 1 and 2 trenches because it ruptured some distance away from the location of the trenches. We find more consistent this second interpretation, as the faulting and deformation style are very similar in both outcrops and because it is very likely that there is a younger reverse fault strand north of Palmar-1 and Palmar-2 trenches of which the intense anthropization of the area has removed any geomorphic evidence.

The oldest surface-rupturing event identified in Buenavista (event Bx, Figure 8) spans a broad time range (32.3 to 5.1 ka) and could be either the same one as the one recorded at Palmar-1 trench (event Pz, 16.4 ka to Cal 9130 B.P.) or a different one. The first option is the simplest, as we have found no evidence of any other surface-rupturing event in Palmar-1 older than 16.4 ka. However, it could be argued that reverse faulting not necessarily always ruptures the surface along the fault trace, so part of the folding affecting Alluvial I sequence in Palmar-1 may be related to an event that did actually produce surface rupture at Buenavista. Additionally, the colluvial deposit at Buenavista (unit D) is very likely associated to different tectonic pulses associated to the growing of the fold, previously to being offset by the oldest surface-rupturing event. These observations suggest that in the period from 32.3 to 5.1 ka there must have been more than one event, chiefly related to folding and blind thrusting. Observations from the estimation of the slip rate of the fault can be used to infer an averaged number of events, as described in the following section.

5.3. Slip Rate of the Carrascoy Fault SW Segment

Estimation of slip rate has been performed by restitution of the top of the Red Unit, dated at 209.1 ± 6.2 ka, from a geological cross section extending from Palmar-1 trench up to the slopes of the Carrascoy Range (Figure 4b). From the total shortening measured (65 ± 15 m) and considering a dip of the fault of 30 ± 10°, an average slip rate of 0.37 ± 0.08 m/kyr is obtained. Additionally, from Buenavista outcrop another estimation is made considering the total displacement estimated for the alluvial sequence on top of unit D (2.2 ± 0.3 m) divided by the age of the overlying unit E (6.9 ± 1.8 ka), yielding an average 0.34 ± 0.09 m/kyr. Both estimations are consistent, even though time bracketing is very different from each other. We prefer the first estimation as it is representative of a longer time period. The obtained slip rate of 0.37 ± 0.08 m/kyr is consistent with the slip rates of the neighboring Alhama de Murcia and Bajo Segura faults, ~0.5 and ~0.2 m/kyr, respectively. In broad terms, it can be observed a decreasing tendency eastward in the slip rate values of these faults, suggesting that the fraction of the Nubia and Eurasian plates convergence absorbed by the ESBZ seems to diminish toward the east and, consistently, most of the convergence would take place along north Algeria.

Considering 0.37 ± 0.08 m/kyr and an average net displacement per event of 1.19 ± 0.14 m calculated from measurements made in the Palmar-1 trench and the Buenavista outcrop, it results a total of 9 to 11 events for the last 30.2 ± 2.1 kyr. It is interesting to note that only the latest three to four of these events may be discriminated at the trenches as surface-rupturing events.

5.4. Seismogenic Potential of Carrascoy Fault SW Segment

The seismogenic potential of a fault can be described in a simple way by the magnitude of the maximum potential earthquake that it can produce, its average recurrence period, and the time elapsed since the last maximum earthquake. The size of such a maximum earthquake can be inferred considering the average displacement per event measured at Buenavista and Palmar-1 trenches (1.19 ± 0.14 m) and the well-known seismic moment equation [*Aki*, 1966] and its relationship to moment magnitude (M_w) [*Hanks and Kanamori*, 1979]. Another approach consists in considering empirical equations on rupture parameters and M_w. Following *Stirling et al*. [2013] recommendations on the use of magnitude-scaling relationships for slow plate boundary reverse faults, we would consider *Stirling et al*. [2008] and *Yen and Ma* [2011], and *Wesnousky* [2008] equations, relating M_w with rupture area and length, respectively.

Either approach first needs to constrain the maximum rupture area of the fault. We have estimated it at 319 ± 46 km^2, considering a surface length of 23 km, and that the Algezares-Casas Nuevas reverse fault merges at depth with the Carrascoy fault. The uncertainties in the dip of the Algezares-Casas Nuevas and Carrascoy

faults, 30° ± 10° and 60° to 90°, respectively, and in the depth of the brittle-ductile transition of the crust in the area, 10 ± 2 km according to *García-Mayordomo* [2005], were taken into account for the rupture area calculation.

Maximum M_w from the equation of seismic moment resulted $M_w = 6.7 \pm 0.1$, which is the same value as the averaged value obtained from the empirical equations described above, $M_w = 6.7 \pm 0.1$. The average recurrence of such an earthquake is then estimated from the ratio of maximum earthquake seismic moment to seismic moment rate from slip rate (0.37 ± 0.08 m/kyr). The resulting estimation, taking into account the standard deviation from all the variables involved, ranges from a maximum 2.3 to a minimum 4.6 kyr, and a mean of 3.3 ± 0.7 kyr. It is worth to note that following this procedure we are assuming that the total seismic moment released by the fault in a seismic cycle equals, basically, to its maximum magnitude seismic moment [*Wesnousky*, 1986]. This estimation is consistent with the average recurrence that can be obtained considering two events in the last 6.0 kyr at Buenavista outcrop. In an earlier work, *García-Mayordomo and Álvarez-Gómez* [2006] estimated for the whole Carrascoy Fault Zone a maximum M_w of 6.8 and a recurrence period ranging from 10,000 to 6000 years. These were preliminary estimations based on literature data and regional mapping, and they are superseded by the present work. Regarding the estimation of the time elapsed since the last major earthquake, we should first look into the earthquake catalog of the area and particularly at the record of known earthquakes felt at the city of Murcia [*IGN-UPM*, 2013], which is located just 4 km north of the Carrascoy fault. The city of Murcia was founded by the Arabs in 850 A.D. and since then it has been a remarkable trade center in the region. Interestingly, only two relevant earthquakes have been felt in Murcia, in 1743 and 1829, reaching a maximum MSK intensity of VII. The latter is the well-known Torrevieja earthquake, attributed to the Bajo Segura fault, 15 km NE to the city of Murcia, which had an estimated M_w 6.3–6.9 and destroyed the town of Torrevieja (I_{EMS} = IX) [*García-Mayordomo and Martínez-Díaz*, 2006; *Alfaro et al*., 2012]. The causative fault of the 1743 earthquake is not known, but considering the relatively low-intensity and inferred magnitude ($M_w = 5.4 \pm 0.8$) [*IGN-UPM*, 2013] of this event, it was not a major earthquake of the Carrascoy Fault. Hence, at least, since 850 A.D. it is very unlikely that the Carrascoy Fault has produced a maximum earthquake, as there would be written records of such an event.

We can infer the number of years that theoretically remain to the next major event if we assume that the youngest event identified in Buenavista took place after 2750 to 2550 B.P. (event Bz, Figure 8) and consider that the recurrence interval between major events is 3.3 ± 0.7 kyr as estimated above. From the different possible outcomes we exclude those not actually credible, which are those that indicate the occurrence of a major event within the last 1164 years, which is the time period between the foundation of the city of Murcia (850 A.D.) and the present (2014), a period in which no major events related to the Carrascoy Fault have been recorded, as explained above. The remaining results indicate that the next major event since 2550 B.P. has not yet taken place and so it could happen in the next ~500 to ~1400 years from Present.

5.5. Recent Geodynamic Evolution of the Carrascoy Fault

First, we present evidence supporting that the Algezares-Casas Nuevas reverse fault formed in the middle-upper Pleistocene progressively from east to west, while simultaneously the Carrascoy strike-slip fault became blocked. Subsequently, we discuss different mechanisms that could explain such evolution.

The U-Th age obtained for the calcrete developed on the top of the Red Unit (circa 217.4 ka) at Palmar-1 trench marks approximately the end of the predominant left-lateral strike-slip tectonics of the SW segment of the Carrascoy Fault Zone (Carrascoy fault), and the onset of a fold-and-thrust system affecting the previous foreland formed by late Neogene and Plio-Quaternary sediments as well as the Quaternary alluvial fan sequences formed by erosion of the former. This fold-and-thrust system progressed northwestward, being the Algezares-Casas Nuevas fault its youngest strand and the current active mountain front in this segment. Simultaneously, the Carrascoy Fault became blocked progressively westward. Thus, a migration of faulting away from the main range occurred since middle-upper Pleistocene. The different arrangement of the drainage and alluvial fan systems between the eastern and western sectors of the segment supports this interpretation (Figure 3). El Cañarico village marks approximately the limit between these contrasting two sectors. At the eastern sector, the incision rate of the outwash streams between the higher mountains and the new relief is stronger than in the western sector. Drainage networks with marked incisions are characteristic of the hanging wall of the thrusts. The erosion rate is also higher at the eastern sector. A few remains of the first generation of alluvial fans are observed in the area between both range fronts. The fan deposits of

the second generation are located north of the recent range front, being this relief the source area of these deposits. Contrastingly, at the western sector, alluvial fans deposits of the first generation are well preserved in the area between both range fronts. The second generation is also located in this same area, coming from the higher mountains. This indicates that at the eastern sector during middle-upper Pleistocene (age of second generation of alluvial fans) the Carrascoy Fault was blocked and the first reverse ruptures reached the surface away from the main range. Meanwhile, at the western sector, the Carrascoy Fault was still active and the deposits of the second generation fans start to onlap the recent relief formed by fault propagation folds related to the birth of the new range front.

Others observations that suggest the progressive growth of the Algezares-Casas Nuevas fault and the simultaneous progressive inactivity of the Carrascoy Fault westward are the height decrease of the recent ridges toward the west and the absence of geomorphological anomalies evidencing the recent left-lateral strike-slip activity of the Carrascoy Fault, as, e.g., left-lateral deflections of the drainage network. This progressive evolution pattern of the SW Segment of the Carrascoy Fault Zone involves a slight change of average strike of the Carrascoy Fault Zone from N050°E (NE Segment) to N065°E (SW Segment), being this last strike more oblique to the regional maximum horizontal compressive stress (Sh_{max}) in this sector of the Betic Cordillera (N170E).

Different geodynamic explanations can be invoked to explain the occurrence of subparallel thrust ruptures separated from the main range and oblique to the regional Sh_{max}:

1. A shift of Sh_{max} from NNW-SSE (N170°E) to NW-SE (N155°E) during the Middle Pleistocene. This is consistent with the recent GPS motions derived from the Quateneo network in the region [*Khazaradze et al*., 2008; *Echeverria et al*., 2011; *Koulali et al*., 2011]; with the current regional convergence between the Eurasian and Nubian plates [*Stich et al*., 2007], and with the observations of *Silva* [1994] who invoked this change to support the interpretation of predominant vertical movements in the E-W trend segments of the Alhama de Murcia and Carrascoy faults. However, *Martínez-Díaz* [2002] argued that this Sh_{max} shift could be simply interpreted as a local stress field change controlled by a local variation of the geometry of the Alhama de Murcia fault, from a NE-SW general trend to a local E-W trend and, therefore, the NNW-SSE Sh_{max} orientation has remained constant since upper Miocene. This general NNW-SSE orientation of the compressive stress field has been recognized along the EBSZ based on different types of stress indicators (borehole breakouts, hydraulic fracturing, fault slip data, and focal mechanism data) and has been interpreted as a local rotation of the present-day NW-SE compressive stress field orientation in the Gibraltar Arc (Betic and Rift alpine chains and the Alboran Sea Basin) [*Fernández-Ibáñez et al*., 2007]. According to these authors, local stress rotations in the Alboran Sea Basin, where there is a flat Moho, provides a clue to confirm that this major strike-slip system (EBSZ) may have a low frictional strength and constitute a major active structure in the complex Nubia-Eurasia plate boundary zone and a stress source in itself.
2. A restraining bend relative to the regional slip vector of the EBSZ structure. The Quaternary activity of the Alhama de Murcia fault decreases northeastward to Alcantarilla village from where it progressively attenuates and is transferred to the parallel Carrascoy Fault system [*Martínez-Díaz et al*., 2012a]. However, the fold-and-thrust system does not seem to extend west of Casas Nuevas village, and so far, we cannot confirm if the Carrascoy system connects to the Alhama de Murcia fault under the sedimentary cover of the Guadalentin depression and so to claim that this structure is a restraining bend.
3. A consequence of deformation partitioning in an oblique left-lateral strike-slip system, but the blockage of the Carrascoy Fault and the subparallel orientation of the Algezares-Casas Nuevas fault respect to the Carrascoy Fault would not support this theory.
4. Finally, we believe that the occurrence of thrusting away from the main range is related to the time evolution of the Carrascoy Fault system. The fold-and-thrust system that defines the Algezares-Casas Nuevas fault is arranged in a left-stepping en echelon pattern increasing the width of the fault zone and suggesting an overall left-lateral component consistent with a positive flower structure. Similar active structures have been described in other oblique strike-slip fault systems worldwide [e.g., *Cunningham et al*., 1997; *Bayasgalan et al*., 1999a, 1999b]. The work of *Bayasgalan et al*. [1999b] outstands particularly because of the similarities with our study area. They studied the Gurvan Bogd Mountains of the Gobi-Altai range (Mongolia) controlled by a system of left-lateral strike-slip faults with a reverse component. Close and subparallel to the main range appear fold-and-thrust systems associated to elongated low ridges,

so-called forebergs [*Florensov and Solonenko*, 1963]. The geomorphology of these fault zones located northwest Artz Bogd Range suggests a similar evolution to what we have observed on the SW segment of the Carrascoy fault. The migration of faulting away from the main range has been observed in many other sites as northern Tien Shan [e.g., *Avouac et al*., 1993] or eastern Iran [e.g., *Walker et al*., 2003]. In all of them, it is likely that this evolution has been driven by stresses associated with topography, which in turn is a consequence of the shortening component.

6. Conclusions

The Carrascoy Fault shows distinct structural and recent tectonics characteristics that strongly suggest its segmentation into two overlapping segments: Los Ramos-El Palmar and Algezares-Casas Nuevas, referred as the NE and SW segments of the Carrascoy Fault Zone, respectively. The differentiation of these two segments dates back to circa 217.4 ka, when the SW segment developed a fold-and-thrust zone with the formation of a new mountain front, diverging northwestward from the former mountain front that was controlled by the Carrascoy fault. The younger fault strand of the Carrascoy Fault SW segment is the Algezares-Casas Nuevas reverse fault. This fault merges at the surface with the overlapping NE segment of the Carrascoy Fault in an area stretching from El Palmar to Algezares villages, where superimposed rupture styles (reverse and strike slip) of both segments have been observed. From Algezares village to the northeast, a single left-lateral strike-slip fault zone is recognized controlling a conspicuous and sharp mountain front, which represents the northeast extension of the Carrascoy Fault and herein called the Carrascoy Fault NE segment.

The onset of the formation of the Algezares-Casas Nuevas fault has been constrained shortly after 217.4 ka. We have discussed different geodynamic contexts that could explain the formation of the new correlative tectonic relief separated from the main range and oblique to the regional Sh_{max}. Based on the similarities of the Algezares-Casas Nuevas fault with the fold-and-thrust systems and elongated low ridges (forebergs) located close and subparallel to the main range described in the Gurvan Bogd Mountains (Gobi-Altai), we suggest that the migration of faulting away from the main range in the SW segment of the Carrascoy Fault Zone has been driven by stresses associated to topographic growth, which in turn is a consequence of the shortening component of the this fault segment.

The maximum potential earthquake magnitude for the SW segment of the Carrascoy Fault Zone has been estimated from different approaches, giving a consistent M_w 6.7 ± 0.1. Considering our slip rate estimation of 0.37 ± 0.08 m/kyr, we have inferred an average recurrence interval between major events of 3.3 ± 0.7 kyr, which is consistent with the value estimated from Buenavista outcrop data. The time of the last surface rupture earthquake is tentatively estimated after 2750 B.P. Assuming that this event occurred shortly after 2750 B.P. the next major earthquake is not expected to happen in the next few centuries. However, this statement has to be taken with caution as more dating analyses are necessary to constraint better the date of the last major earthquake of the Carrascoy Fault, as well as the uncertainty of the estimated average recurrence interval, and the usual nonperiodic behavior of seismogenic faults. The Carrascoy Fault represents a major earthquake hazard to the city of Murcia and its large metropolitan area, where more than half a million people live, thus justifying the need to carry on with further studies on its recent tectonics and paleoseismology.

Acknowledgments
The original laboratory data regarding dated samples for this paper is available in the supporting information in Tables S1–S5. This work was supported by SISMOGEN (IGME, 2279) and FASEGEO (CGL2009-09726) research projects and a technical assistance of the Civil Protection Service of Murcia. The authors greatly appreciate the carefully revision of J.M. Azañón and J. Cabral that lead to an improved version of the manuscript.

References

Aki, K. (1966), Generation and propagation of G waves from the Niigata earthquake of June 16, 1964. II., Estimation of earthquake movement, release energy, and stress–strain drop from G waves spectrum, *Bull. Earthquake Res. Inst.*, *44*, 23–88.

Aldaya, F., F. Alvarez, J. Galindo-Zaldivar, F. González-Lodeiro, A. Jabaloy, and F. Navarro-Vilá (1991), The Maláguide-Alpujárride contact (Betic Cordilleras, Spain): A brittle extensional detachment, *C. R. Acad. Sci. Paris*, *313*, 1447–1453.

Alfaro, P. (1995), Neotectónica en la Cuenca del Bajo Segura (Extremo oriental de la Cordillera Bética) PhD thesis, Universidad de Alicante, Alicante, 218 pp.

Alfaro, P., R. Bartolomé, M. J. Borque, A. Estévez, J. García-Mayordomo, F. J. García-Tortosa, A. J. Gil, E. Gràcia, C. Lo Iacono, and H. Perea (2012), The Bajo Segura Fault Zone: Active blind thrusting in the Eastern Betic Cordillera (SE Spain), *J. Iberian Geol.*, *38*(1), 271–284.

Amores, R., J. L. Hernández-Henrile, and J. J. Martínez-Díaz (2001), Sobre los factores relacionados con la evaluación de la peligrosidad sísmica en la Región de Murcia paper presented at 2nd Congreso Iberoamericano de Ingeniería Sísmica, Asociación Española de Ingeniería Sísmica, Madrid.

Amores, R., J. L. Hernández-Henrile, and J. J. Martínez-Díaz (2002), Estudio gravimétrico previo aplicado a la identificación de fallas ocultas como fuentes sismogénicas en la Depresión del Guadalentín (Región de Murcia), *Geogaceta*, *32*, 307–310.

Argus, D. F., R. G. Gordon, and C. DeMets (2011), Geologically current motion of 56 plates relative to the no-net-rotation reference frame, *Geochem. Geophys. Geosyst.*, *12*, Q11001, doi:10.1029/2011GC003751.

Avouac, J. P., P. Tapponnier, M. Bai, H. You, and G. Wang (1993), Active thrusting and folding along the northeastern Tien Shan, and rotation of Tarim relative to Dzungaria and Kazakhstan, *J. Geophys. Res.*, *98*, 6755–6804.

Azañón, J. M., and A. Crespo-Blanc (2000), Exhumation during a continental collision inferred from the tectonometamorphic evolution of the Alpujarride Complex in the central Betics (Alboran Domain, SE Spain), *Tectonics*, *19*, 549–565.

Azañón, J. M., A. Crespo-Blanc, and V. García-Dueñas (1997), Continental collision, crustal thinning and nappe forming during the pre-Miocene evolution of Alpujarride Complex (Alboran Domain, Betic), *J. Struct. Geol.*, *19*, 1055–1071.

Azañón, J. M., V. García-Dueñas, and B. Gotte (1998), Exhumation of high-pressure metapelites and coeval crustal extension in the Alpujarride Complex (Betic Cordillera), *Tectonophysis*, *285*, 231–252.

Balanyá, J. C., and V. García-Dueñas (1987), Les directions structurales dans le Domaine d'Alborán depart et d'autre duDétroit de Gibraltar, *C. R. Acad. Sci. París*, *304*, 929–933.

Bardají, T., J. L. Goy, N. A. Mórner, C. Zazo, P. Silva, L. Somoza, C. Dabrio, and J. Baena (1995), Towards a Plio-Pleistocene chronostratigraphy in the eastem Betic Basins (SE Spain), *Geod. Acta*, *8–2*, 112–126.

Bayasgalan, A., J. Jackson, J. F. Ritz, and S. Carretier (1999a), Field examples of strike-slip fault terminations in Mongolia and their tectonic significance, *Tectonics*, *18*, 394–411.

Bayasgalan, A., J. Jackson, J. F. Ritz, and S. Carretier (1999b), "Forebergs", flower structures, and the development of large intra-continental strike-slip faults: The Gurvan Bogd fault system in Mongolia, *J. Struct. Geol.*, *21*, 1285–1302.

Bell, J. W., F. Amelung, and G. C. P. King (1997), Preliminary late quaternary slip history of the Carboneras fault, Southeastern Spain, *J. Geodyn.*, *24*(1–4), 51–66.

Boccaletti, M., R. Gelati, A. C. López-Garrido, G. Papani, J. Rodríguez-Fernández, and C. Sanz de Galdeano (1987), Neogene-Quaternary sedimentary-tectonic evolution of the Betic Cordillera, *Acta Nat. l'Ateneo Parmense*, *23*(41), 179–200.

Bousquet, J. C. (1979), Quaternary strike-slip faults in southern Spain, *Tectonophysics*, *52*, 277–286.

Buontempo, L., and A. Wuestefeld (2013), Complex fault structure interactions of crustal shear zones revealed by seismic anisotropy: An example in the eastern betic cordillera (Spain), *Terra Nova*, *25*(1), 57–64.

Calmel-Avila, M. (2002), The Librilla rambla, an example of mophogenetic crisis in the Holocene (Murcia, Spain), *Quat. Int.*, *93–94*, 101–108.

Calmel-Avila, M., P. G. Silva, T. Bardají, J. L. Goy, and C. Zazo (2009), Drainage system inversion in the Guadalentín Depression during the Late Pleistocene-Holocene (Murcia, Spain), in *Advances in Studies on Desertification*, edited by C. Romero et al., pp. 461–464, Servicio de Publicaciones Universidad de Murcia, Murcia, Spain.

Cunningham, W. D., B. F. Windley, L. A. Owen, T. Barry, D. Dorjnamjaa, and J. Badamgarav (1997), Geometry and style of partitioned deformation within a late Cenozoic transpressional zone in the eastern Gobi-Altay Mountains, Mongolia, *Tectonophysics*, *277*, 285–306.

De Larouzière, F., C. Montenat, P. Ott O'Estevou, and P. Griveaud (1987), Evolution simultanée des basin néogènes en compression et en extension dans un couloir de décrochement: Hinojar et Malarron (Sud Est de l'Espagn), *Bull. Centre Rech. Explor. Prod. Elf-Aquitaine*, *11*, 23–38.

De Larouzière, F., J. Bolze, P. Bordet, J. Hernyez, C. Montenat, and P. Ott D'Estevou (1988), The Betic segment of the litospheric Trans-Alboran shear lone during the late Miocene, *Tectonophysics*, *152*, 41–52.

Dirección General de Protección Civil (DGPC), Civil Protection Special Plan for Seismic Risk at the Region of Murcia (SISMIMUR) (2006), *Dirección General de Protección Civil [in Spanish]*, Consejería de Presidencia, Comunidad Autónoma de la Región de Murcia, Murcia, Spain.

Echeverria, A., G. Khazaradze, J. Garate, E. Asensio, E. Masana, and E. Suriñach (2011), Present-day GPS crustal deformation rates in the Eastern Betics (SE. Spain) Geophysical Research Abstracts 13, EGU2011, EGU General Assembly 2011, Viena, −8005.

Egeler, C., and O. J. Simon (1969), Orogenic evolution of the betic zone (Betic cordilleras, Spain) with emphasis on the nappe structure, *Geol. Mijnbouw*, *48*, 295–305.

Fernández-Ibáñez, F., J. I. Soto, M. D. Zoback, and J. Morales (2007), Present-day stress field in the Gibraltar Arc (western Mediterranean), *J. Geophys. Res.*, *112*, B08404, doi:10.1029/2006JB004683.

Florensov, N. A., and V. P. Solonenko (Eds.) (1963), The Gobi-Altay earthquake. Akademiya Nauk USSR Moskow (in Russian; English translation by Israel Program for Scientific Translations, U.S. Department of Commerce, Washington, DC, 1965).

Frizon de Lamotte, D., J. J. Jarrige, and J. C. Vidal (1980), Le magmatisme bético-rifain est-illié aune zone d'accidents en décrochement "Trans-Albarán"? R.A.S.T. Marseille, Soc. Géol. France, Marseille.

Galindo-Zaldívar, J., F. González-Lodeiro, and A. Jabaloy (1989), Progressive extensional shear structures in a detachment contact in the Western Sierra Nevada (Betic Cordilleras, Spain), *Geod. Acta*, *3*(1), 73–85.

García-Dueñas, V., J. C. Balanyá, and J. M. Martínez-Martínez (1992), Miocene extensional detachments in the outcropping basement of the Northern Alboran Basin (Betics) and their Tectonic Implications, *Geo Mar. Lett.*, *12*, 88–95.

García-Mayordomo, J. (2005), Caracterización y análisis de la peligrosisdad sísmica en el sureste de España.) PhD thesis, Universidad Complutense de Madrid, Madrid.

García-Mayordomo, J., and J. A. Álvarez-Gómez (2006), Estimación del terremoto máximo posible y su intervalo de recurrencia en la Falla de Carrascoy (Murcia) para su implementación en el cálculo de la peligrosidad sísmica de la región, *Geogaceta*, *39*, 51–54.

García-Mayordomo, J., and J. J. Martínez-Díaz (2006), Caracterización sísmica del Anticlinorio del Bajo Segura (Alicante): Fallas del Bajo Segura, Torrevieja y San Miguel de Salinas, *Geogaceta*, *40*, 19–22.

García-Mayordomo, J., J. M. Gaspar-Escribano, and B. Benito (2007), Seismic hazard assessment of the Province of Murcia (SE Spain): Analysis of source contribution to hazard, *J. Seismol.*, *11*, 453–471, doi:10.1007/s10950-007-9064-0.

García-Mayordomo, J., et al. (2012), The Quaternary Active Faults Database of Iberia (QAFI v.2.0), *J. Iberian Geol.*, *38*(1), 285–302.

Gaspar-Escribano, J. M., B. Benito, and J. García-Mayordomo (2008), Hazard-consistent response spectra in the Region of Murcia (Southeast Spain): Comparison to earthquake-resistant provisions, *Bull. Earthquake Eng.*, *6*, 179–196, doi:10.1007/s10518-007-9051-4.

Goy, J. L., C. Zazo, L. Somoza, C. J. Dabrio, and T. Bardaji (1989), Litoral Béticas Orientales (Alicante, Murcia, Almería), in *Libro Guía Excursión B-I, Litoral Mediterráneo, 2nd Reu. Cuaternario Ibérico, Sec. Publ.*, edited by C. Zazo et al., 99, ETS Ingenieros Industriales, Madrid.

Hanks, T. C., and H. Kanamori (1979), A moment-magnitude scale, *J. Geophys. Res.*, *84*, 2348–2350.

Heaton, T. J., P. G. Blackwell, and C. E. Buck (2009), A Bayesian approach to the estimation of radiocarbon calibration curves: The IntCal09 methodology, *Radiocarbon*, *51*(4), 1151–64.

Hernández-Enrile, J. L., and J. J. Martínez-Díaz (2001), Using travertine deformations to characterize paleoseismic activity along an active oblique-slip fault: The Alhama de Murcia fault (Betic Cordillera, Spain), *Acta Geol. Hispánica*, *36*(3–4), 297–313.

Herrero, M. J., J. M. Insua-Arevalo, J. Garcia-Mayordomo, and R. Martin-Banda (2014), Pleistocene calcrete deposits from southern Spain as indicators of climatic conditions and tectonic activity, Geophysical Research Abstracts Vol. 16, EGU2014-12130-1, EGU General Assembly 2014, held 27 April - 2 May, 2014 in Vienna, Austria.

Ibarra, P., F. M. Rubio, J. García-Mayordomo, R. Martín-Banda, E. Rodríguez-Escudero, and A. Salazar (2012), Detección y caracterización de fallas activas mediante tomografía de resistividad, in *Proceedings of the 7ª Asamblea Hispano Portuguesa de Geodesia y Geofísica*, edited by J. Zurutuza, San Sebastián.

Instituto Geológico y Minero de España (IGME) (2012), QAFI: Quaternary Active Faults Database of Iberia, [accessed 2014/07/07, Available from IGME. [Available at http://www.igme.es/infoigme/aplicaciones/QAFI/.]

Instituto Geográfico Nacional-Universidad Politécnica de Madrid (IGN-UPM) (2013), *Actualización de Mapas de Peligrosidad Sísmica de España 2012*, Centro Nacional de Información Geográfica, Madrid.

Insua-Arévalo, J. M., J. García-Mayordomo, A. Salazar, E. Rodríguez-Escudero, R. Martín-Banda, J. A. Álvarez-Gómez, C. Canora, and J. J. Martínez-Díaz (2015), Paleoseismological evidence of Holocene activity of the Los Tollos Fault (Murcia, SE Spain): A lately formed Quaternary tectonic feature of the Eastern Betic Shear Zone, *J. Iberian Geol.*, *41*(3), 333–350.

Jabaloy, A., J. Galindo-Zaldívar, and F. González-Lodeiro (1993), The Alpujarride-Nevado-Filabride extensional shear zone Betic Cordillera SE Spain, *J. Struct. Geol.*, *15*, 555–569.

Jerez, F., F. Leyva, F. J. García-Tortosa, and P. Cabra (2015), Geological Map of Spain, Sheet 933-Alcantarilla, scale 1:50.00, IGME, Madrid, 197 p.

Khazaradze, G., J. Gárate, E. Suriñach, J. M. Davila, and E. Asensio (2008), Crustal deformation in south-eastern Betics from CuaTe-Neo GPS network, *Geo-Temas*, *10*, 1023–1026.

Koulali, A., D. Ouazar, A. Tahayt, R. W. King, P. Vernant, R. E. Reilinger, S. McClusky, T. Mourabit, J. M. Davila, and N. Amraoui (2011), New GPS constraints on active deformation along the Africa–Iberia plate boundary, *Earth Planet. Sci. Lett.*, *308*, 211–217.

Leyva, F., C. Sanz de Galdeano, F. J. García-Tortosa, and P. G. Silva (2010), Geological mapping and memory, in *Mapa Geológico de España*, sheet 934-Murcia, scale 1:50.000, Spanish Geological Survey, Madrid.

Marín-Lechado, C., F. J. Roldán-García, A. Pineda-Velasco, P. Martínez-Zubieta, J. Rodero-Pérez, and G. Díaz-Pinto (2011), Mapa Geológico Digital continuo E. 1: 50.000, Zonas internas de las Cordilleras Béticas (Zona-2100), in *GEODE: Mapa Geológico Digital continuo de España [on line]*, *Sistema de Información Geológica Continua: SIGECO*, edited by J. Navas, IGME, [Accessed 2014/07/07, available from IGME. [Available at http://cuarzo.igme.es/sigeco/default.htm.]

Martínez-Díaz, J. J. (2002), Stress field variation related to fault interaction in a reverse oblique-slip fault: The Alhama de Murcia fault, Betic Cordillera, Spain, *Tectonophysics*, *356*, 291–305.

Martínez-Díaz, J. J., M. A. Rodríguez-Pascua, R. Pérez-López, J. García-Mayordomo, J. L. Giner-Robles, F. Martín-González, M. Rodríguez-Peces, J. A. Álvarez-Gómez, and J. M. Insua-Arévalo (2011), Informe geológico preliminar del terremoto de Lorca del 11 de mayo del año 2011, 5.1 Mw, Tech. Rep., 46 pp., Geological Survey of Spain, IGME, Madrid.

Martínez-Díaz, J. J., E. Masana, and M. Ortuño (2012a), Active tectonics of the Alhama de Murcia fault, Betic Cordillera, Spain, *J. Iberian Geol.*, *38*(1), 253–270.

Martínez-Díaz, J. J., J. A. Álvarez-Gómez, J. García-Mayordomo, J. M. Insua-Arévalo, F. Martín-González, and M. J. Rodríguez-Peces (2012b), Interpretación tectónica de la fuente del terremoto de Lorca de 2011 (MW 5,2) y sus efectos superficiales, *Bol. Geol. Min.*, *123*(4), 441–458.

Masana, E., J. J. Martínez-Díaz, J. L. Hernández-Enrile, and P. Santanach (2004), The Alhama de Murcia fault (SE Spain), a seismogenic fault in a diffuse plate boundary: Seismotectonic implications for the Ibero-Magrebian region, *J. Geophys. Res.*, *109*, B01301, doi:10.1029/2002JB002359.

Masana, E., E. Gràcia, X. Moreno, R. Bartolomé, and J. J. Dañobeitia (2010), Characterizing the seismic potential of the Eastern Betics Shear Zone (EBSZ), a major source of earthquakes in Southeastern Iberia, in *Contribución de la Geología al Análisis de la Peligrosidad Sísmica*, edited by J. M. Insua-Arévalo and F. Martín-González, pp. 101–104, Sigüenza, Guadalajara (España).

Medialdea, A., K. J. Thomsen, A. S. Murray, and G. Benito (2014), Reliability of equivalent-dose determination and age-models in the OSL dating of historical and modern palaeoflood sediments, *Quat. Geochronol.*, *22*, 11–24.

Montenat, C. (1973), Les formations Neógenes el Quaternaires du Levant espagnol, PhD thesis, Univ. Paris, Orsay.

Montenat, C. (1977), Les bassins néogènes et quaternaires du Levant d'Alicante à Murcie (Cordillères bétiques orientales, Espagne). Stratigraphie, paléontologie et evolution dynamique, *Docum. Lab. Géol. Fac. Sci. Lyon*, *69*, 1–345.

Montenat, C., P. Ott D'Estevou, and P. Masse (1987), Tectonic-sedimentary characters of the betics Neogene basins evolving in a crustal transcurrent shear zone (SE Spain), *Bull. Centre Rech. Explor Prado Elf-Aquitaine*, *11*, 1–22.

Moreno, X. (2010), Neotectonic and paleoseismic onshore-offshore integrated study of the Carboneras Fault (Eastern Betics, SE Iberia), PhD thesis, Universitat de Barcelona, Spain.

Moreno, X., E. Masana, E. Gràcia, R. Bartolomé, and O. Piqué-Serra (2008), Estudio paleosismológico de la Falla de Carboneras: Evidencias tierra-mar de actividad tectónica reciente, *Geo-Temas*, *10*, 11,035–1038.

Oeschger, H., U. Siegenthaler, U. Schotterer, and A. Gugelmann (1975), A box diffusion model to study the carbon dioxide exhange in nature, *Tellus*, *27*, 168–92.

Ortuño, M., E. Masana, E. García-Meléndez, J. J. Martínez-Díaz, P. Stêpancikvá, P. P. Cunha, R. Sohbati, C. Canora, J. P. Buylaert, and A. S. Murray (2012), An exceptionally long paleoseismic record of a slow-moving fault: The Alhama de Murcia fault (Eastern Betic shear zone, Spain), *Geol. Soc. Am. Bull.*, *124*(9–10), 1474–1494.

Ott D'Estevou, P., and C. Montenat (1985), Evolution structurale de la zone bétique orientale (Espagne) du Tortonien à l'Holocène, *C. R. Acad. Sci. Paris II*, *300*, 363–368.

Perea, H., E. Gràcia, P. Alfaro, R. Bartolomé, C. Lo Iacono, X. Moreno, E. Masana, and E. V. E. N. T.-S. H. E. L. F. Team (2012), Quaternary active tectonic structures in the offshore Bajo Segura basin (SE Iberian Peninsula–Mediterranean Sea), *Nat. Hazards Earth Syst. Sci.*, *12*, 3151–3168, doi:10.5194/nhess-12-3151-2012.

Reimer, P. J., et al. (2009), IntCal09 and Marine09 radiocarbon age calibration curves, 0–50,000 years cal BP, *Radiocarbon*, *51*(4), 1111–50.

Sanz de Galdeano, C. (1983), Los accidentes y fracturas principales de las Cordilleras Béticas, *Estud. Geol.*, *43*, 435–443.

Sanz de Galdeano, C. (1990), Geologic evolution of the Betic Cordilleras in the Western Mediterranean. Miocene to the present, *Tectonophysics*, *172*, 107–119.

Sanz de Galdeano, C., A. C. López-Garrido, and F. J. García-Tortosa (1998), Nuevos datos para la estimación de los valores de levantamiento desde el Tortoniense Superior a la actualidad en la parte centro-occidental de la Sierra de Carrascoy (provincia de Murcia), *Geogaceta*, *23*, 139–142.

Serpelloni, E., G. Vannucci, S. Pondrelli, A. Argnani, G. Casula, M. Anzidei, P. Baldi, and P. Gasperini (2007), Kinematics of the western Africa-Eurasia plate boundary from focal mechanisms and GPS data, *Geophys. J. Int.*, *169*(3), 1180–1200, doi:10.1111/j.1365-246X.2007.03367.x.

Silva, P. G. (1994), Evolución Geodinámica de la depresión del Guadalentín (Murcia) desde el Mioceno Superior hasta la actualidad: Neotectónica y Geomorfología, PhD thesis, Universidad Complutense de Madrid, Madrid.

Silva, P. G., A. M. Harvey, C. Zazo, and J. L. Goy (1992a), Geomorphology, depositional style and morphometric relationships of Quaternary alluvial fans in the Guadalentín Depression (Murcia, SE Spain), *Z. Geomrphol.*, *36–3*, 661–673.

Silva, P. G., J. L. Goy, and C. Zazo (1992b), Discordancias progresivas y desarrollo geomorfológico de abanicos aluviales en la Depresión del Guadalentín (SE de España), *Geogaceta*, *11*, 67–70.

Silva, P. G., J. L. Goy, L. Somoza, C. Zazo, and T. Bardaji (1993), Landscape response to strike-slip faulting linked to collisional settings: Quaternary tectonics and basin formation in the Eastern Betics (SE Spain), *Tectonophysics*, *224*, 289–303.
Silva, P. G., J. L. Goy, C. Zazo, and T. Bardají (2003), Fault-generated mountain fronts in southeast Spain: Geomorphologic assessment of tectonic and seismic activity, *Geomorphology*, *50*, 203–225.
Silva, P. G., M. Calmel-Avila, T. Bardaji, J. L. Goy, and C. Zazo (2008), Transition from alluvial to fluvial systems in the Guadalentin Depression (SE. Spain) during the Holocene. Lorca Fan versus Guadalentín River, *Geomorphology*, *100*, 144–153.
Soria, J. M., P. Alfaro, A. Ruiz-Bustos, and F. Serrano (1996), Organización estratigráfica y bioestratigráfica del Plioceno en el borde sur de la Cuenca del Bajo Segura (sector de Rojales, Alicante), Cordillera Bética Oriental, *Estud. Geol.*, *52*, 137–145, doi:10.3989/egeol.96523-4261.
Stich, D., J. B. Martín, and J. Morales (2007), Deformación sísmica y asísmica en la Zona Béticas-Rift-Alborán, *Rev. Soc. Geol. España*, *20*(3–4), 311–319.
Stirling, M. W., M. C. Gerstenberger, N. J. Litchfield, G. H. McVerry, W. D. Smith, J. Pettinga, and P. Barnes (2008), Seismic hazard of the Canterbury region, New Zealand: New earthquake source model and methodology, *Bull. N. Z. Natl. Soc. Earthquake Eng.*, *41*, 51–67.
Stirling, M. W., T. Goded, K. Berryman, and N. Litchfield (2013), Selection of earthquake scaling relationships for seismic-hazard analysis, *Bull. Seismol. Soc. Am.*, *103*(6), 1–19, doi:10.1785/0120130052.
Stuiver, M., and T. F. Braziunas (1993), Modeling atmospheric 14C influences and 14C ages of marine samples to 10,000 BC, *Radiocarbon*, *35*(1), 137–89.
Thomsen, K. J., M. Jain, L. Bøtter-Jensen, A. S. Murray, and H. Jungner (2003), Variation with depth of dose distributions in single grains of quartz extracted from an irradiated concrete block, *Radiat. Meas.*, *37*, 315–321.
Thomsen, K. J., A. S. Murray, L. Bøtter-Jensen, and J. Kinahan (2007), Determination of burial dose in incompletely bleached fluvial samples using single grains of quartz, *Radiat. Meas.*, *42*(3), 370–379.
Vegas, R., L. M. Barranco, and J. T. Vázquez (1987), Tectónica de bloques en el SE de España: Aplicación de la teledetección a un límite de placas de tipo intracontinental, *Geogaceta*, *3*, 17–19.
Walker, R., J. Jackson, and C. Baker (2003), Surface expression of thrust faulting in eastern Iran: Source parameters and surface deformation of the 1978 Tabas and 1968 Ferdows earthquake sequences, *Geophys. J. Int.*, *152*, 749–765.
Wesnousky, S. G. (1986), Earthquakes, Quaternary faults, and seismic hazard in California, *J. Geophys. Res.*, *91*, 12,587–12,631.
Wesnousky, S. G. (2008), Displacement and geometrical characteristics of earthquake surface ruptures: Issues and implications for seismic hazard analysis and the process of earthquake rupture, *Bull. Seismol. Soc. Am.*, *98*(4), 1609–1632.
Yen, Y.-T., and K.-F. Ma (2011), Source-scaling relationship for M 4.6–8.1 earthquakes, specifically for earthquakes in the collision zone of Taiwan, *Bull. Seismol. Soc. Am.*, *101*(2), 464–481.